Treatment with sodium butyrate has therapeutic benefits for Machado-Joseph disease through the induction of autophagy

Maxinne Watchon*, Katherine J. Robinson*, Luan Luu*, Kristy C. Yuan, Albert Lee, Flora Cheng, Emily K. Don, Garth A. Nicholson, Angela S. Laird^

Centre for Motor Neuron Disease Research, Department of Biomedical Science, Faculty of Medicine, Health and Human Sciences, Macquarie University, Sydney, NSW Australia

*These authors contributed equally

^Corresponding author: Dr. Angela Laird, Faculty of Medicine, Health and Human Sciences Level 1, 2 Technology Place, Macquarie University, NSW 2109, Australia
angela.laird@mq.edu.au

Abstract

Machado-Joseph disease (MJD) is a fatal neurodegenerative disease caused by expansion of the trinucleotide repeat region within the *ATXN3/MJD* gene. Mutation of *ATXN3* causes formation of neurotoxic ataxin-3 protein aggregates, neurodegeneration and motor deficits. Here we investigated the therapeutic potential of sodium butyrate (SB), the sodium salt of butyric acid, a metabolite naturally produced by gut microbiota, on cultured SH-SY5Y cells and transgenic zebrafish expressing human ataxin-3 containing 84 glutamine (Q) residues to model MJD. MJD SH-SY5Y cells were found to contain ataxin-3 oligomeric species and protein aggregates. Interestingly, treatment with SB decreased the size of detergent-insoluble ataxin-3 aggregates *in vitro*. Further investigation revealed that SB treatment increased activity of the autophagy protein quality control pathway in the MJD cells and decreased presence of ataxin-3 oligomers in an autophagy-dependent manner. Treatment with SB was also beneficial *in vivo* through induction of autophagy and improving swimming performance in transgenic MJD zebrafish. Co-treating the MJD zebrafish with SB and chloroquine, an autophagy inhibitor, prevented the beneficial effects of SB, suggesting that the improved swimming performance was autophagy-dependent . Furthermore, intraperitoneal injection of SB to wild type mice resulted in increased levels of neuronal LC3B levels, indicating induction of autophagy within the brain. Collectively, our findings suggest that SB can induce activity of the autophagy pathway and can produce beneficial effects *in vitro* and *in vivo*. We propose that treatment with sodium butyrate warrants further investigation for the treatment of neurodegenerative diseases underpinned by proteinopathy mechanisms, including MJD.

Keywords

Autophagy, Machado-Joseph disease, neurodegeneration, polyQ, Spinocerebellar ataxia 3, sodium butyrate, zebrafish, trinucleotide repeat disease, flow cytometry, microbiota

Abbreviations

MJD, Machado-Joseph disease; HDAC, histone deacetylase; polyQ, polyglutamine; SB, sodium butyrate; dpf, days post fertilization; EGFP, enhanced green fluorescent protein; FSC, forward scatter signal; H3K9, acetylated histone 3 at lysine 9; H4K5, acetylated histone 4 at lysine 5

Introduction

Machado-Joseph disease (MJD), also known as spinocerebellar ataxia-3, is a neurodegenerative disease characterized by a progressive loss of muscle control and movement, leading to wheelchair dependence and decreased lifespan [1]. Clinical symptoms of MJD include ataxia, dystonia, rigidity, muscle atrophy and visual and speech disorders [1-3]. MJD is the most common of the hereditary ataxias found throughout the world (21-28% of autosomal-dominant ataxia) [4-6], with a high prevalence within the Azores of Portugal [7] and Indigenous communities of north east Arnhem Land in Australia [8].

MJD is caused by inheritance of an expanded CAG repeat region within the *MJD1/ATXN3* gene on chromosome 14 [9-11]. Whilst the *ATXN3* gene of healthy subjects contains a short CAG trinucleotide repeat region (12-40 CAG repeats), this region contains over 40, and as high as 87, CAG repeats in MJD patients [7, 9, 12, 13]. The *ATXN3* gene encodes the ataxin-3 protein, with the CAG repeat region encoding a polyglutamine (polyQ) tract towards the C-terminus of the protein [12, 13]. Neuropathological staining of patient brain samples often reveals the presence of neuronal intranuclear inclusions (NII) containing the ataxin-3 protein [2, 14, 15] and extraction of these proteins has revealed the presence of full-length ataxin-3 protein, as well as smaller ataxin-3 protein fragments [16].

Whilst the function of the ataxin-3 protein is not fully understood it is known to function as a deubiquitinating (DUB) enzyme [1] and can affect levels of transcription through interactions with co-activators and histones [17-19]. It has been previously reported that ataxin-3 is a histone binding protein and that polyQ expansion within the protein increases

the extent of that binding, in turn affecting histone acetylation [17]. Furthermore, it has also been suggested that mutated polyQ proteins can also inhibit the function of histone acetyltransferase [20-22]. Indeed, cell culture and animal models, such as drosophila and transgenic mice expressing polyQ expanded human ataxin-3, have been reported to have histone hypoacetylation [21, 23, 24]. However, this histone hypoacetylation has not been reported to be present in all models of the disease [20].

One therapeutic strategy that has been explored for MJD is treatment with drugs that may increase levels of histone acetylation, called histone deacetylase (HDAC) inhibitors. HDACs are a class of enzymes that remove acetyl groups from ε-N-acetyl lysine located on histones, causing histones to bind DNA more tightly and prevent transcription [25, 26]. Previous studies have reported that treatment with HDAC inhibitors can have neuroprotective effects for the treatment of MJD [20, 21, 23, 24, 27], and other neurodegenerative diseases including Huntington's Disease and Alzheimer's disease [28-31]. Compounds with this HDAC inhibitor capacity include suberoylanilide hydroxamic acid (SAHA), trichostatin A, resveratrol, valproic acid and sodium butyrate [25, 32-36].

Sodium butyrate (SB), is a sodium salt of butyric acid, which is a short-chain fatty acid that is produced within the gut by intestinal microbiota during fermentation of undigested dietary carbohydrates and fiber [26, 37]. Whilst butyric acid is critical for intestinal homeostasis, it also exerts a wider range of effects including inhibition of cell proliferation, downregulation of pro-inflammatory effectors, repression of gene expression and HDAC inhibition, resulting in increased acetylation of histones 3 and 4 [24, 37]. As SB can elicit such a wide spectrum of positive effects, it is likely SB has multiple distinct mechanisms of action [37, 38], many of which are yet to be fully elucidated.

In this study, we aimed to determine the efficacy of SB in alleviating MJD pathology in cell culture and zebrafish models of MJD. Furthermore, we aimed to elucidate the underlying mechanism by which SB rescues MJD disease phenotypes. Enhancing our understanding of the mechanisms of action underlying the neuroprotective effects induced by SB could provide therapeutic implications for a wide range of neurodegenerative and proteinopathy diseases. We hypothesized that, in addition to rectifying transcriptional dysregulation, SB can ameliorate MJD phenotypes via induction of the autophagy protein quality control pathway. Increased activation of the autophagy pathway may act to degrade or remove pathological ataxin-3 oligomeric species or aggregates in cell cultures, alleviating

neurotoxicity. Importantly, here we demonstrate that administration of SB can induce autophagy and decrease MJD disease phenotypes both *in vitro* and *in vivo*, highlighting the therapeutic potential of autophagy inducers in MJD and other related neurodegenerative diseases.

Results

MJD models recapitulate phenotypes found in human MJD patients, including presence of protein aggregates and histone hypoacetylation

Immunostaining of neuron-like (neuroblastoma, SH-SY5Y) cells stably expressing human ataxin-3, or an empty vector control, showed expression of ataxin-3 throughout the cytoplasm and nucleus of the cell (Fig. 1A-C). Immunostaining also revealed the presence of cytoplasmic ataxin-3 positive puncta in cells expressing ataxin-3-28Q and -84Q (Fig. 1B-C; white arrows). Further examination revealed co-localization of ataxin-3 puncta with ubiquitin in ataxin-3-84Q cells, recapitulating a pathological hallmark found in the brains of MJD patients (Fig. 1D). Automated quantification of the number of potential ataxin-3 protein aggregates (puncta with a diameter of 2.25-20 μm) revealed that cells stably expressing ataxin-3-84Q had more puncta than cells expressing ataxin-3-28Q or an empty vector control (Fig. 1E).

To further characterize the presence of increased protein aggregates in MJD cells, wild type SH-SY5Y cells were transiently transfected with EGFP-fused human ataxin-3-84Q, EGFP-fused human ataxin-3-23Q or an EGFP-only vector control. Transfected cells underwent flow cytometric analysis to quantify the number and size of Triton-X insoluble GFP^+ aggregates. Firstly, the number of GFP^+ cells per sample were calculated by comparing the number of GFP^+ particles (cells) to the total number of cells (determined by a 4',6-diamidino-2-phenylindole [DAPI] stain for nuclei). Similar cell (DAPI) counts were present in all lysed samples (Supp. Fig 1A). The number of Triton-X insoluble EGFP-positive aggregates was then identified by treating the samples with 0.5% Triton-X followed by flow cytometry, an approach termed FloIT [39]. The number of Triton-X insoluble GFP positive particles was then expressed relative to the number of GFP positive cells per sample. This revealed a greater number of insoluble particles in cells expressing GFP-ataxin-3 84Q compared to the empty vector control (Fig. 1F), aligning with immunostaining findings. Additionally, EGFP-ataxin-3-84Q cells harbored larger insoluble particles (based on the forward scatter, FSC, signal) (Supp. Fig. 1B). Triton-X insoluble

GFP^+ particles were then compared with calibration beads to approximate size, revealing an increased mean diameter of insoluble GFP^+ particles in ataxin-3-84Q expressing cells compared with an empty vector control (mean: 19.90 ± 0.828 µm versus 14.13 ± 1.075 µm respectively; Fig. 1G).

Immunoblot analysis of SH-SY5Y cells stably expressing human ataxin-3 or an empty vector control revealed the expression of endogenous ataxin-3, ataxin-3-28Q and ataxin-3-84Q at appropriate sizes (45kDa, 50kDa and 65kDa respectively, Fig. 1H). Expression of ataxin-3 monomers did not differ between ataxin-3 28Q and ataxin-3 84Q cells, but as expected, was greater than in the empty vector control cells (Fig. 1I). However, cells expressing ataxin-3-84Q were found to contain an additional ataxin-3 band, at approximately 140kDa, suggesting the formation of an ataxin-3 dimer, which was not present in cells expressing ataxin-3-28Q (Fig. 1J). We identified the dimeric ataxin-3 84Q by comparing the location of the immunoreactive band of dimeric ataxin-3 on the immunoblot with a Coomassie stained 1D SDS PAGE gel that was run in parallel to the immunoblot. This region was excised, in-gel trypsin digestion was performed, and tryptic peptides were analyzed by LC-MS/MS. We confirmed that this immunoreactive band was indeed dimeric ataxin-3 84Q (Supp. Fig. 2, Supp. Table 1).

Previously, we developed a transgenic zebrafish model of MJD with the intent to screen drug candidates for the treatment of MJD [40]. As the ataxin-3 protein is known to be functionally involved in transcriptional regulation through binding of transcriptional co-activators to histones, we sought to investigate the status of acetylated histone 3 at lysine 9 (H3K9) and acetylated histone 4 at lysine 5 (H4K5) in the 6 day-old MJD zebrafish. Zebrafish transgenically expressing EGFP-tagged human ataxin-3-84Q travel significantly shorter distances than non-transgenic larvae or those expressing EGFP-ataxin-3-23Q during motor testing (escape response to darkness assay) [40]. Immunoblots confirmed that 6dpf transgenic zebrafish expressed human ataxin-3 protein of appropriate sizes (72kDa and 84kDa for EGFP-ataxin-3 23Q and 84Q respectively), as well as endogenous zebrafish ataxin-3 (34kDa; Fig. 2A). Furthermore, smaller ataxin-3-positive cleavage fragments were also present, consistent with our previous findings [40]. We found that at 6dpf, EGFP-ATAXIN-3-84Q larvae displayed decreased expression of both H3K9 (Fig. 2B) and H4K5 (Fig. 2C) when compared to non-transgenic controls. This suggests expansion of the polyQ region within the ataxin-3 protein may affect the acetylation status of histones 3 and 4 in MJD zebrafish. In contrast, we found that SH-SY5Y cells stably expressing ataxin-3-84Q

yielded decreased expression of H3K9 compared to the ataxin-3 28Q expressing cells, however similar levels of H4K5 were detected across examined genotypes (Supp. Fig. 3).

Treatment with sodium butyrate increases histone acetylation and alters the aggregation profile of MJD cell culture models

To investigate the therapeutic potential of sodium butyrate (SB), we analyzed whether SH-SY5Y cells stably expressing human ataxin-3-84Q displayed increased histone acetylation following SB treatment (3 mM for 72 hours). Immunoblotting for the acetylated histones 3 and 4 (acetylated H3K9 and H4K5 respectively, Fig. 3A) revealed that SB treatment produced an increase in both H3K9 and H4K5 (Fig. 3B, C). Treatment with SB, compared to vehicle treated cells, was also found to decrease the number of ataxin-3 aggregates by 30% as revealed by ataxin-3 immunostaining (Fig. 3D, E). Furthermore, flow cytometric analysis revealed a significant reduction in the average size of detergent insoluble GFP^+ particles after 24 hours of SB (3 mM) treatment in cells transiently expressing EGFP-ataxin-3-84Q (Fig. 3F). Interestingly, levels of the polyQ expanded ataxin-3 specific dimers decreased with SB treatment (Fig. 3G, H), suggesting the induction of a protein quality control pathway.

Treatment with sodium butyrate rectifies the histone hypoacetylation and improves swimming of MJD zebrafish

EGFP-ataxin-3-84Q zebrafish were treated with SB (250 µM, 500 µM and 1 mM) between 24 hours post fertilization (hpf) and 6dpf to determine whether hypoacetylated histone levels could be rectified. Indeed, immunoblotting for acetylated H3K9 and H4K5 revealed a dose dependent increase in levels of acetylated of histone 3 and histone 4 with SB treatment, rectifying the hypoacetylation previously observed in MJD zebrafish (Fig. 4A). This was confirmed when quantifying the amount of acetylated H3K9 following treatment with 500 µM and 1 mM SB (Fig. 4B) and acetylated H4K5 from 1 mM SB (Fig. 4C), compared to the vehicle control. Next, we examined whether SB treatment could prevent motor impairment displayed in the mutant ataxin-3 zebrafish at 6dpf. Examination of the movement of the zebrafish during the escape response to darkness motor assay revealed, as reported previously, that zebrafish expressing ataxin-3 with polyglutamine expansion swam shorter distances than non-transgenic controls, and treatment with SB produced a dose-dependent increase of this distance (Fig. 4D, E).

Sodium butyrate treatment induces autophagy and aids removal of protein aggregates in MJD SH-SY5Y Cells

We next investigated the mechanisms by which SB was reducing the presence of ataxin-3 protein aggregates. To investigate whether the autophagy protein quality control pathway was involved do this, we performed immunostaining on SH-SY5Y cells expressing ataxin-3 84Q after treatment with either SB (3 mM for 72 hours) and/or an autophagy inhibitor, bafilomycin A1 (3 mM 72 hours of SB treatment, 100 nM in for the final for 2 hours prior to immunostaining for ataxin-3 and LC3B). Co-staining for ataxin-3 and LC3B enabled the examination of colocalization of ataxin-3 aggregates (arrow) with autophagosomes (arrow) (Fig. 5A). In vehicle control treated cells, LC3B and ataxin-3 puncta colocalize and this interaction is less apparent in SB and SB/bafilomycin A1 co-treated cells. However, this may be due to the reduction in ataxin-3 aggregates in SB treated cells (Fig. 5B). Bafilomycin A1 treatment alone did not change the colocalization of ataxin-3 aggregates and autophagosomes when compared to vehicle control (Fig. 5A), but bafilomycin A1 cotreatment appeared to reinstate the ataxin-3 positive protein aggregates. Automated image analysis of the number of ataxin-3 positive aggregates (size threshold: diameter of 2.25 to 20 μm) within ataxin-3-84Q expressing cells revealed that SB treatment significantly decreased the number of ataxin-3 aggregates, but a two-hour bafilomycin A1 treatment at the end of the SB treatment did not prevent this decrease (Fig. 5B). Unfortunately, longer SB and bafilomycin A1 co-treatment experiments were found to be toxic in this cell model (data not shown).

To examine whether SB treatment was causing oligomeric species of ataxin-3 to be removed via autophagy, immunoblots containing protein lysates of the SH-SY5Y cells expressing ataxin-3 84Q treated with either SB (3 mM for 72 hours) and/or bafilomycin A1 (3 mM 72 hours of SB treatment, 100 nM in for the final for 2 hours prior to protein extraction), probed with a marker of autophagosomes, LC3, marker for autophagic flux, sequestesome-1 (p62) and ataxin-3 (Fig. 5C). LC3 is known marker of autophagosomes, where LC3 conjugation from LC3I to LC3II represents the maturation of autophagosome[41]. Immunoblotting of cells co-treated with SB and bafilomycin A1 displayed an increased LC3II/LC3I ratio when compared to each treatment individually, indicating that SB was inducing the autophagy pathway (Fig. 5C, D). When comparing the effect of drug treatments on levels of p62, a marker of autophagic flux, SB treatment was

found to significantly affect decrease p62 levels (Fig. 5C, E). However, treatment with bafilomycin A1 alone increased p62 levels compared to SB-treatment alone and SB/bafilomycin A1 co-treatment (Fig. 5C, E). Immunoblots from mutant MJD SH-SY5Y cells showed that SB treatment significantly affected ataxin-3 proteinopathy (Fig. 5C). SB treatment, regardless of bafilomycin treatment, decreased dimeric ataxin-3 levels compared to the vehicle treated control (Fig. 5F). However, bafilomycin treatment in the final two hours of SB treatment did not prevent the decreased ataxin-3 dimer levels produced by the SB treatment (Fig. 5F).

Flow cytometric analysis was used to confirm whether SB treatment, after 24 hours, affected the quantity or size of insoluble GFP^+ ataxin-3 particles. Representative flow cytometric scatter plots revealed the presence of insoluble GFP^+ particles in all treatment groups, however the relative size of each population (as indicated by the forward scatter, FSC, signal) was shifted to the left in cells exposed to SB treatment (Fig. 6A). Surprisingly, SB treatment was in fact increasing the number of insoluble GFP^+ particles when compared with vehicle treatment, bafilomycin A1 treatment alone and co-treatment of SB and bafilomycin A1. Next, we compared the size of detergent insoluble GFP^+ particles to beads of a known diameter. In contrast to the number of insoluble GFP^+ particles, SB treated cells harbored insoluble particles with a smaller mean diameter compared to vehicle treatment (Fig. 6C). A similar effect was also observed when vehicle treatment was compared to SB/bafilomycin A1 co-treatment. Collectively, these findings suggest that SB treatment may increase the total number of insoluble particles as larger particles may be broken down into multiple smaller particles, consequently causing an increase in the overall number of insoluble aggregates detected when compared to vehicle treatment.

To confirm that the reduction of dimeric ataxin-3 species was mediated by SB-induced autophagy, SH-SY5Y ataxin-3 84Q cells were co-treated with SB (3 mM) and an autophagy inhibitor, 3MA (5 mM) for 72 hours (Fig. 7A). Whilst SB treatment decreased the amount of ataxin-3 dimer present compared to vehicle control, co-treatment with SB and 3MA together resulted in no decrease in the amount of ataxin-3 dimer compared to vehicle-treated (Fig. 7C). This suggests 3MA prevented the capacity of SB to decrease ataxin-3 dimers and that changes in ataxin-3 proteinopathy were dependent on SB-mediated autophagy.

Sodium butyrate treatment induces the autophagy pathway in the transgenic MJD zebrafish and improves swimming in an autophagy-dependent manner

To confirm that autophagy was indeed being induced by SB treatment *in vivo*, the transgenic MJD zebrafish were treated between 1-6 dpf with either SB alone (1 mM), vehicle alone, an autophagy inhibitor (chloroquine, 1.5 mM or 3 mM) alone or co-treated with SB and chloroquine . Protein lysates of groups of larvae from these treatment groups were then subjected to western blot analysis and probed for LC3B and ataxin-3 (Fig. 8A). Densiometric analysis revealed that SB treatment alone produced similar levels of LC3II to vehicle treated larvae (Fig. 8B). In contrast, chloroquine treatment (both 1.5 mM and 3 mM) alone, like bafilomycin A1 treatment in the ataxin-3-84Q SH-SY5Y cells, produced an increase in LC3II levels when compared to vehicle treatment. Lastly, co-treatment with SB and 3 mM chloroquine produced a further increase in LC3II levels, when compared to all other groups, including 3 mM chloroquine alone (Fig. 8B). The finding of increased LC3II levels following co-treatment with SB and chloroquine when compared to 3 mM chloroquine alone indicates that autophagy is being induced upstream of the autophagy blockade produced by chloroquine. Taken together, these findings confirm that autophagy was induced in the MJD zebrafish by the SB treatment.

To confirm that the improved swimming phenotype of the MJD zebrafish produced by SB treatment was due to the induction of autophagy, we performed a co-treatment experiment followed by motor behavior analysis. The MJD zebrafish larvae were treated with SB (1 mM), chloroquine (1.5 mM), or both, from 1-6 dpf, prior to motor tracking. Treatment with SB alone again resulted in an increase in the distances swum by the MJD zebrafish, compared to vehicle treatment, whilst the addition of 1.5 mM chloroquine to SB treatment prevented this improvement in motor function (Fig. 8C, D). Whilst immunoblotting data suggests that our higher dose of chloroquine (3 mM) is more effective at inhibiting autophagy than the lower dose (1.5 mM), preliminary motor behavior experiments revealed impaired swimming performance in non-transgenic control larvae following treatment with 3 mM chloroquine (1-6 dpf, Supp. Fig 4). Thus, whilst 3 mM chloroquine treatment is more effective at inhibiting autophagy, this treatment regime produced confounding effects in movement assays. As such, the lower dose of 1.5 mM chloroquine was selected for all movement assay experiments in order to reduce any potential confounding effects. Indeed, we found no differences in the distance swum by vehicle treated EGFP-ataxin-3 84Q larvae and larvae treated with 1.5 mM of chloroquine alone, suggesting the concentration of chloroquine chosen was not inducing toxicity (Fig. 8D). This indicates that chloroquine

treatment was able to suppress the beneficial effect of SB, and therefore that the beneficial effect of SB treatment was indeed autophagy dependent.

Systemic administration of sodium butyrate can induce autophagy within the murine brain

To further complement our existing *in vivo* data, we tested whether repeated intraperitoneal (i.p.) administration of 200 mg/kg sodium butyrate could induce autophagy within the brains of wild type (non-transgenic) mice (Fig. 9A). Western blotting of whole mouse brain protein lysates revealed that male mice treated with SB displayed increased levels of LC3B compared to vehicle controls (Fig. 9B-C). We also tested whether there were any differences in the expression of acetylated histones 3 and 4 (H3K9 and H4K5 respectively). Treatment with 200 mg/kg SB (IP) did not result in increased levels of H3K9 and H4K5 compared to vehicle controls, suggesting that SB treatment time may not have been sufficient to affect histone acetylation (data not shown).

Discussion

In vitro cell culture models recapitulate neuropathological hallmarks of human MJD

Firstly, we reported that neuronal-like (neuroblastoma) SH-SY5Y cells expressing ataxin-3 containing a polyQ expansion (84 polyQ repeats) developed ataxin-3 positive aggregates. We also demonstrated these ataxin-3 aggregates were co-localized with ubiquitin positive puncta. These findings align with existing experimental evidence that suggests polyglutamine expanded ataxin-3 can form ubiquitinated protein aggregates within cultured murine or human neuroblastoma cells [14, 42, 43] and reports of intraneuronal ataxin-3 positive inclusions in MJD brain tissue [14, 15, 44, 45].

Next, we aimed to determine if we could employ the high-throughput flow cytometric analysis approach, FloIT, to quantify the number and size of insoluble ataxin-3 particles in MJD cells. This method has been previously utilized to investigate TDP-43, SOD1 and huntingtin-positive inclusions *in vitro* [39]. FloIT analysis revealed the presence of Triton-X insoluble, ataxin-3 positive aggregates that were larger in size in ataxin-3-84Q expressing cells. To our knowledge, we are the first to report a flow cytometric approach to investigate the number and size of detergent-insoluble ataxin-3 aggregates. Furthermore, our flow cytometry findings are consistent with existing reports of ataxin-3 aggregate

formation and size, aligning with findings from Weishäupl et al [46] that demonstrate that cultured cells transiently transfected with human ataxin-3 constructs can develop ataxin-3 positive aggregates within 24 hours. Interestingly, Weishäupl et al [46] did not detect a significant difference in the number of aggregates present at 24-hours post transfection in cells expressing ataxin-3 with a short polyQ chain and cells expressing ataxin-3 with a long polyQ chain, conflicting with the present findings. However, this may be due to the methodological approach employed by Weishäupl and colleagues, as microscopy approaches may lack the sensitivity required to detect ataxin-3 aggregates at this time point.

In addition to ataxin-3-positive aggregates, we also found evidence of ataxin-3 oligomeric species resembling ataxin-3 dimers, found exclusively in cells expressing polyQ expanded ataxin-3. Several cell culture and animal models of neurodegenerative diseases such as Parkinson's disease, Alzheimer's disease and Huntington's disease have demonstrated cytotoxicity of soluble oligomeric α-synuclein, amyloid β and huntingtin protein, respectively [47-57]. When considered together, our cell culture model of MJD recapitulates disease phenotypes present in MJD patients, confirming the appropriateness of our cell culture model for investigating disease mechanisms and the mechanisms of efficacious therapeutics.

Sodium butyrate increases activity of the autophagy protein quality control pathway

In the present study, we aimed to further elucidate the neuroprotective effects of SB treatment. Whilst the therapeutic efficacy of SB has previously been demonstrated in preclinical animal models of MJD and other neurodegenerative diseases [22, 24, 38], we aimed to explore the mechanisms or pathways activated by SB that facilitate amelioration of MJD disease phenotypes. Indeed, our cell culture data suggested that SB was acting to modulate the aggregation profile and overall proteinopathy of ataxin-3-84Q expressing cells. Therefore, we hypothesized that SB acted to enhance the activity of protein recycling pathways, such as the autophagy protein quality control pathway. Treatment with autophagy inducer compounds has previously been demonstrated to aid the clearance of polyQ expanded ataxin-3 or huntingtin and reduce related cellular toxicity [40, 42, 58-65]. In particular, clearance of polyglutamine containing mutant huntingtin aggregates via autophagy has shown to reduce toxicity and prevent neuronal dysfunction [60-65].

Indeed, we found that prolonged (72 hr) treatment of the MJD cells with SB resulted in decreased levels of ataxin-3 dimers and aggregated forms of ataxin-3, as identified by

ataxin-3 immunostaining. Our immunofluorescent staining of SH-SY5Y cells expressing ataxin-3-84Q confirmed the co-localization of ataxin-3 aggregates with autophagosomes in vehicle control treated cells, indicating that ataxin-3 aggregates are targeted for degradation via autophagy. Colocalisation of protein aggregates and autophagosomes has also been reported to occur in other neurodegenerative diseases including other polyglutamine diseases such as spinocerebellar ataxia-7 and Huntington's disease, Alzheimer's disease, amyotrophic lateral sclerosis and Parkinson's disease [66-69]. Whilst SB treatment caused the co-localization of ataxin-3 aggregates and autophagosomes to become less apparent, this is likely due to the decrease in ataxin-3 aggregates detected by the immunostaining following SB treatment.

Furthermore, we identified that SB treatment was inducing autophagy, indicated by increased LC3II/LC3I ratio in SB treated cells following blockage of autophagy with the autophagy inhibitor, bafilomycin A1. Whilst bafilomycin A1 co-treatment for the final 2 hours of SB treatment was not sufficient to prevent removal of dimers and protein aggregates by SB, blockage of autophagy with an alternative compound, 3MA, throughout the SB treatment period, prevented the decrease in Ataxin-3 dimers produced by SB treatment. This finding aligns with a previous report by Qiao et al [70] that SB treatment induced autophagy in enteroendocrine cells expressing α-synuclein. However, our finding is the first evidence of SB removing oligomeric species or protein aggregates in a neuronal-like cell line through demonstrated activity of the autophagy pathway.

Our novel flow cytometry investigation of MJD cell cultures likely provides further evidence to support this finding. In our flow cytometric analysis of insoluble aggregates, following a shorter period of SB treatment (24 hours), we found that SB was acting to increase the number of detergent insoluble ataxin-3 particles. This finding was surprising and seemed to refute our immunostaining results. However, analysis of the size of the insoluble protein aggregates revealed that SB treatment had decreased the mean diameter of the insoluble particles. Whilst blocking autophagosome-lysosome fusion with bafilomycin A1 at the end of the SB treatment period failed to prevent the effect of SB on aggregate size and number, this is likely due to the fact that SB-induced breakdown of ataxin-3 aggregates could not be prevented by bafilomycin within such a short timeframe.

Interestingly, the relationship between ataxin-3 aggregate size and toxicity has previously been examined, with findings from Simões et al [71] suggesting increased toxicity of large

ataxin-3 aggregates when compared with smaller aggregates. Whilst our finding of increased protein aggregates following treatment with SB was initially surprising, when considered together, these data suggest that sodium butyrate is in fact inducing macroautophagy as insoluble ataxin-3 particles are being broken down into multiple smaller insoluble particles. We therefore conclude that 24-hour SB treatment is sufficient to reduce aggregate size, however extended SB treatment (72 hours) is required for complete removal and clearance of ataxin-3 aggregates.

Recently, Santana et al [42] explored the effects of trehalose, a known autophagy inducer, in two mouse models expressing expanded ataxin-3. Interestingly, the authors found that 72-hour treatment with 10 mM trehalose increased autophagosome production and reduced the size of ataxin-3 aggregates, but failed to reduce the number of ataxin-3 aggregates suggesting lack of aggregate removal and clearance [42]. Whilst the role of ataxin-3 protein aggregates in MJD neuropathology is still debated [72, 73], experimental evidence suggests that the type and conformation of ataxin-3 aggregates may contribute more to toxicity than mere presence of aggregates [42, 46, 71, 74].

A further extension of this finding was our demonstration that SB treatment is also capable of inducing autophagy *in vivo* within MJD zebrafish and wild type mice. To our knowledge, the present study is the first reported *in vivo* evidence of SB inducing autophagy and autophagy-dependent improvements in motor function to treat a neurodegenerative disease. The findings from our murine brain analysis are also of importance, as these findings highlight that systemic administration of SB can cross the blood-brain barrier and induce autophagy within the brain. These findings could have significant therapeutic implications for the future treatment of neurodegenerative diseases, as treatments that aid clearance of toxic protein aggregates or oligomeric species within the brain may reduce overall neurotoxicity and slow down neurodegeneration.

Interestingly, previous studies investigating the therapeutic potential of SB in neurodegenerative models, including a mouse model of Huntington's disease [38] and an in vitro model of Parkinson's disease [70], found no effect of SB treatment on the number of protein aggregates, conflicting with the present study. One exception is that SB treatment on of a SOD1G93A mice mouse model of amyotrophic lateral sclerosis detecting reported a reduction in SOD1 positive aggregates in the colon compared to vehicle treated animals, however the same was not reported for neurons [75]. Despite this, they did not report

whether SOD1 protein aggregates were reduced within neurons, or whether the autophagy pathway was induced by SB treatment. The One explanation for why this finding has not been reported previously is that the optimal dose of SB required to induce autophagy may be relatively narrow or it may vary depending on specific protein quality control impairments induced by the individual gene mutations. Indeed, Minamiyama et al [22] found lower doses of SB were required to ameliorate neuropathology in a mouse model of SBMA in comparison to doses that were found to be efficacious in a transgenic mouse model of Huntington's disease [38]. Further studies are required to confirm whether SB can induce degradation of ataxin-3 protein aggregates found within the brain of MJD animal models.

Sodium butyrate ameliorates histone hypoacetylation and movement deficits in zebrafish

We also report that our previously reported MJD zebrafish (EGFP-ataxin-3 84Q) [40] displayed hypoacetylation of histones 3 and 4 compared to non-transgenic control zebrafish at 6 days post fertilization. This is consistent with ataxin-3 protein having a role transcriptional regulation [17, 20, 76] and previous reports of expression of polyQ expanded ataxin-3 resulting in histone hypoacetylation [23, 24]. Furthermore, we found that treatment with SB rectified this imbalance, increasing acetylation of both histones 3 and 4. An increase in levels of acetylated histone 3 and 4 produced by the SB treatment is an indication of histone deacetylase (HDAC) inhibition.

These findings contribute to existing evidence that suggests amelioration of histone hypoacetylation through HDAC inhibition can improve motor phenotypes in polyQ diseases. Other studies treating mice models of MJD with SB are in alignment with our findings [21, 76]. The transgenic MJD mice developed by Chou and colleagues show a motor phenotype, neuropathology and hypoacetylation of histone 3 and histone 4. Chronic treatment of MJD mice with SB restored movement performance, to similar to wild type controls, with notable improvements in latency to fall, locomotor activity, foot dragging and dendritic arborisation induced by the mutant ataxin-3 [24]. This study also shows a rescuing of hypoacetylated histones 3 and 4. HDAC inhibition is currently being explored as a potential treatment for a range of neurodegenerative diseases, including Huntington's disease, Alzheimer's disease and Parkinson's disease [77].

Multiple protective mechanisms have been proposed to result from treatment with compounds with HDAC inhibitor activity. These include regulation of transcription and in turn increased plasticity, neuronal regeneration, increased levels of neurotrophic factors such as GDNF and BDNF, restoration of balance to cerebellar circuitry and even protection against glutamate-induced excitotoxicity [21, 25, 78, 79]. Our findings demonstrate that induction of autophagy is another therapeutic benefit of treatment with the HDAC inhibitor compound SB. Multiple other HDAC inhibitor compounds, such as sodium valproate and resveratrol, have similarly been demonstrated to induce autophagy [80-84]. Whether the autophagy activity is dependent on the HDAC inhibitor activity, and the mechanism of any linkage, is yet to be determined.

Concluding Remarks

Sodium butyrate treatment was found to affect the aggregation status of polyQ expanded ataxin-3 *in vitro*, decreasing presence of ataxin-3 oligomers and enhancing degradation of ataxin-3 positive aggregates. The present study also provides the first experimental evidence of sodium butyrate treatment inducing increased autophagic activity *in vivo* in a model of neurodegenerative disease. Induction of the autophagy protein quality control pathway may be a therapeutic option for neurodegenerative diseases due to potential to increase the clearance and degradation of toxic protein species such as mutant ataxin-3 protein. Further, our findings suggest that sodium butyrate can rectify histone hypoacetylation and prevent the development of movement phenotypes in transgenic MJD, presenting the first evidence of HDAC inhibition rescuing disease phenotypes in a zebrafish model of neurodegenerative disease.

These findings have relevance to a broad range of neurodegenerative diseases as there is growing evidence to suggest that changes to the gut microbiome, and therefore changes to levels of metabolites released by the gut, such as butyric acid, may impact on the function of the nervous system [26, 70]. This is because, whilst butyric acid is naturally produced in the gut, there is evidence to suggest that it can travel from the gut and penetrate the blood-brain barrier, eliciting effects via the gut-brain axis [26, 70]. Our findings suggest a potential mechanism by which these disruptions may have an effect on the development or treatment of neurodegenerative disease. We propose that our findings that treatment with SB can induce autophagy, both *in vitro* and *in vivo*, resulting in protective effects such as preventing the development of impaired movement are important for research into

treatment for MJD and related diseases. These results indicate that sodium butyrate and butyric acid both warrant further investigation as autophagy inducing agents with therapeutic potential for a wide range of neurodegenerative and proteinopathy diseases.

Methods

Transgenic MJD zebrafish

All animal experiments were performed in accordance with the Animal Ethics Committee of Macquarie University, N.S.W., Australia (ARA: 2016/004 and 2017/019). Zebrafish were housed in a standard recirculating aquarium system at 28.5^{o}C. These experiments used our previously described transgenic zebrafish model of MJD [40]. Briefly, the driver lines express a HuC (*elav*) neuronal promoter [85] driving Gal4 VP16 [Tg(elav3:GAL4-VP16-mCherry)mq15], and the responder lines express EGFP-ATXN-3 (containing 23 or 84 CAG repeats) and dsRED under the control of the UAS promoter that is activated only in tissues that are expressing Gal4 VP16 [Tg(UAS:Hsa.ATXN3_23xCAG-EGFP,DsRed)mq16 and Tg(UAS:Hsa.ATXN3_84xCAG-EGFP,DsRed)mq17]. For the studies described here driver and responder lines were mated to generate F1 HuC-EGFP-Ataxin-3 23Q or 84Q lines, which were in-crossed to generate F2 embryos for use in this study.

MJD Cell culture model

SH-SY5Y cells were grown in Dulbecco's Modified Eagle's Medium (DMEM)/Nutrient Mixture F12 Ham supplemented with 10% fetal bovine serum (FBS) and maintained at 37^{o}C and 5% CO_2. A pcDNA3.1 vector containing full length ataxin-3 (28Q or 84Q) and a neomycin resistant gene was used for stable selection of transfected cells. 500 µg/mL of neomycin was used to select cells stably expressing ATAXIN--3. Cells were treated with 250 µg/mL of neomycin (Sigma) to maintain expression of the selective expression of the ataxin-3 gene or vector control.

Drug treatments in MJD cell cultures and transgenic MJD zebrafish

SH-SY5Y cells stably expressing human ataxin-3 were seeded into a 24-well plate at a density of 40,000 cells/cm^2 and incubated at 37^{o}C supplemented with 5% CO_2. 24 hours after seeding, cells were treated with SB (3 mM, Cayman Chemicals [Cat #13121]) or vehicle control (autoclaved water) diluted in growth media for a total of 72 hours, with SB-

containing media replenished every 24 hours to ensure drug efficacy. For the co-treatment study with an autophagy inhibitor bafilomycin A1 (100 nM dissolved in DMSO, Roche) was added for the final 2 hours of SB treatment or cells were pre-treated with 3MA (5mM, Cayman Chemicals) for 1 hour before SB was added and left on for the duration of the SB treatment. For the zebrafish drug treatment studies, zebrafish embryos (1 day post fertilization; dpf) were screened for fluorescence (EGFP and dsRED) indicating that they were positive for the EGFP-ataxin-3 transgenes. In the drug treatment groups, positive embryos were treated for five days with SB (250 μM, 500 μM and 1 mM, solubilized in milliQ water). Appropriate volumes of SB were then diluted in zebrafish E3 media, with the control group containing only E3 media [86]. Co-treatment with SB and the autophagy inhibitor chloroquine (1.5 mM and 3 mM, Sigma-Aldrich [Cat# C6628], solubilized in milliQ water) was performed in the same manner but with chloroquine stock solution added to the E3 media containing sodium butyrate so that the solution also contained either 1.5 mM or 3 mM chloroquine. Vehicle treated groups were left in E3 medium.

Zebrafish motor behavior testing

Motor function assays were performed as described in Watchon et al [40]. All behavioral tracking was performed using a ZebraLab Tracking System (ZebraBox; Viewpoint). Tracking of 6dpf larvae were conducted in 24 multi-well plates within the ZebraBox housed with an enhanced light source, under conditions of 6 minutes light, 4 minutes dark and 4 minutes light. The total distance travelled by each larva within the dark phase was calculated.

Repeated acute drug treatments in wild-type mice

Eight male C57/Bl6 mice (20-28 g upon arrival) were obtained from Australian BioResources (Mossvale, NSW, Australia). All rodent experiments were conducted in accordance with the Australian Code of Practice for the Care and Use of Animals for Scientific Purposes (8th Edition, 2013) and were approved by the Macquarie University Animal Ethics Committee (2017/044). Animals were group-housed (four animals per cage) in exhaust ventilated cages (125mm (W) x 350mm (L) x 135mm (H)) in a temperature and light controlled room (21 $\pm$ 1^{o} C, 12-hour light/dark cycle). Mice were provided environmental enrichment and food and water were available *ad libitum* in home cages.

Animals were acclimated for seven days and then randomly allocated to receive intraperitoneal injection of either vehicle or sodium butyrate. Sodium butyrate was dissolved in 0.9% isotonic saline at a dose of either 200mg/kg and injected at a volume of 5 mL/kg of body weight. Vehicle administration consisted of 0.9% isotonic saline solution. IP injections were performed daily for three consecutive days during the light cycle. Animals were euthanized 60 minutes post-final IP injection via an injection of sodium pentobarbitone (110 mg/2 mL, IP). Once heavily anaesthetized, brains were removed and rapidly frozen in liquid nitrogen. All samples were stored at –80 ^{o}C until processing.

Western blotting

SH-SY5Y cells stably expressing human ataxin-3 (28Q and 84Q), were washed with ice cold PBS and incubated in 100 µL of RIPA buffer containing protease inhibitors (Complete ULTRA tablets, Roche). Cells were gently agitated on orbital shaker for five minutes before being spun down at 18000g for 15 minutes. Protein lysates were prepared from zebrafish larvae (6 dpf) in RIPA buffer containing protease inhibitors (Roche), using a manual dounce. For analysis of mouse brain tissue, one hemisphere of brain was lysed in RIPA buffer (volume = 5 x wet weight of brain tissue) containing protease inhibitors (Roche). Tissue was homogenised using a hand homogeniser and probe sonicator. Homogenates were centrifuged for 30 minutes at 15000g. Supernatants were collected and measured for protein concentration using the Pierce™ BCA Protein Assay Kit (Thermo Fisher Scientific).

Equal amounts of protein were separated using SDS-PAGE and transferred to PVDF membrane for immunoblot probing. Antibodies used included rabbit anti-MJD (kind gift from H. Paulson), mouse anti-GAPDH (Proteintech). To test the effect of drug treatments, immunoblots were probed for anti-rabbit acetylated histone 3 at lysine 9 and histone 4 at lysine 5 (H3K9 and H4K5 respectively, Cell Signaling), anti-rabbit LC3B (Abcam), and anti-rabbit p62 (Abcam). The immunoblots were probed with appropriate secondary antibodies (Promega and Li-Cor) and visualised by chemiluminescence (Supersignal detection kit, Pierce) using a BioRad GelDoc System or fluorescent detection using the LiCor Odyssey CLX. The intensity of bands within the immunoblot were quantified by Image Studio Lite and the target protein expression level was determined by normalizing against the loading control protein.

Immunofluorescence staining of cell culture

Cultured cells were fixed with 4% paraformaldehyde and permeabilization with 3% BSA blocking buffer containing 0.075 – 0.2% Triton-X 100 for 10-20 minutes. Cells were blocked for one hour with phosphate buffered saline (PBS) containing 3% BSA then incubated with primary antibodies overnight at 4^{o}C. These antibodies consisted of anti-mouse ataxin-3 (Millipore, 1:500), anti-rabbit LC3B (Abcam, 1:500) and anti-rabbit ubiquitin (ThermoFisher, 1:1000). Coverslips were washed 3x for five minutes with PBS then incubated in secondary antibodies (anti-mouse Alexa Fluor 488, anti-rabbit Alexa Fluor 555) for one hour at room temperature. Coverslips were washed 3x for five minutes with PBS then mounted with Prolong Gold with DAPI (Thermo).

Immunostained cells were imaged under epifluorescence (Zeiss AxioImager Z2 microscope 40x objective lens running ZEN 2011) at consistent exposure times. Confocal images were acquired using an Inverted Zeiss LSM 880 microscope using 63X objective with 1-2% laser power. Quantification of ataxin-3 positive aggregates was conducted using Fiji [87].

Flow cytometric analysis of insoluble ataxin-3

For flow cytometry experiments, SH-SY5Y cells were transiently transfected with human ATXN3 plasmids containing a fluorescent tag. Human ATXN3 cDNA was subcloned into a pCS2+ vector to generate ATXN3 constructs containing a short polyQ (28Q) and an expanded polyQ (84Q) fluorescently tagged with EGFP.

SH-SY5Y cells were cultured in DMEM/Ham's Nutrient Mixture F12 and supplemented with 10% FBS and 5% CO_2. Cells were seeded into 6-well plates and incubated at 37^{o}C. Once cells had reached 85% confluency (24-48 hours), cells were transiently transfected with 1 µg of DNA/3.5cm^2 using Lipofectamine 2000 (ThermoFisher, Catalogue # 11668030). Cells were treated with vehicle or 3 mM SB for 24 hours, with transfected cells treated with 100 nM bafilomycin A1 for the final two hours prior to harvesting.

To determine transfection efficiency, live cells were imaged within 6-well plates at 10x magnification using an EVOS FL monochrome microscope (Invitrogen, catalogue # AMF4300) running Invitrogen image acquisition software. Cells were harvested using 0.5% trypsin/EDTA and pelleted (1500 rounds per minute, 5 minutes at room temperature [RT]). Cells were re-suspended in 500 µL of lysis buffer (PBS containing 1% Triton-X 100 and complete protease inhibitors [Roche]). DAPI was added to lysis buffer (final concentration 5 µM) and incubated at RT for 5 minutes, protected from light.

Flow cytometry was performed using a Becton Dickson Biosciences LSR Fortessa analytical flow cytometer and calibrated using CST beads (Becton Dickson). The fluorescence of transfected cells was compared to an untransfected control sample. Lysed samples were analyzed by plotting forward scatter (area) against relative DAPI (379-28-A) or EGFP (530-30-A/535) fluorescence. Forward scatter threshold was set at 200 to minimize exclusion of small insoluble particles [39]. A total of 20 000 events were acquired with all axes set to $\log_{10}$. Nuclei were identified and gated based on intensity of UV fluorescence and relative size (forward scatter). The number of insoluble GFP particles, indicating insoluble ataxin-3 particles, was analyzed based on GFP fluorescent intensity and forward scatter [39]. Gating of Triton-X insoluble GFP^+ positive particles was performed by comparing populations to an untransfected control sample. For analysis comparing the number of insoluble particles across SH-SY5Y cells expressing different ataxin-3 constructs, the FloIT equation was employed whereby the number of insoluble GFP^+ particles was divided by the number of detected nuclei x the transfection efficiency [39]. For analysis comparing the effect of different drug treatments, the FloIT equation was not employed as treatment with sodium butyrate and bafilomycin A1 were hypothesized to alter the amount of ataxin-3 expression within transfected cells and thus altering GFP intensity, potentially confounding transfection efficiency analysis. Therefore, for analysis comparing the effect of drug treatments on SH-SY5Y cells expressing ataxin-3-84Q, data was analyzed as the number of insoluble GFP^+ particles divided by the number of detected nuclei. Drug-induced effects were presented as the fold change differences when compared to vehicle treated controls. Mean insoluble GFP^+ particle size diameter was calculated for each group by calculating the overall mean forward scatter value for GFP^+ populations in each treatment group, then comparing this value to the mean forward scatter value of fluorescent calibration beads with a known diameter (ThermoFisher, catalogue # F13838). All flow cytometric analysis and gating was performed using FlowJo (version 10.6.2, Becton Dickson Biosciences).

In-gel Trypsin Digestion and Liquid Chromatography Mass spectrometry (LC-MS)

SH-SY5Y cell lysates expressing ATXN3-84Q were separated in 4-12% NuPAGE Bis-Tris polyacrylamide gels (Invitrogen) in duplicate gels. One gel was Coomassie stained and de-stained in 7% acetic acid, 10% methanol while the second gel was transferred to nitrocellulose membrane and western blot analysis for ATXN3 was performed. Fraction 1-7 in the Coomassie stained gel were identified by comparison with the molecular weight of

the ataxin-3-84Q band from the western blot results. The bands in the gel were excised and cut into 1-2 mm pieces and de-stained in 50 mM ammonium bicarbonate pH 8, followed by 50 mM ammonium bicarbonate/50% acetonitrile pH 8. The de-stained gel pieces were dehydrated in 100% acetonitrile and the solution was removed to allow gel pieces to air dry. The proteins were reduced and alkylated with 10 mM dithiothreitol (DTT) and 20 mM iodoacetamide (IAA) respectively and digested with trypsin (12.5 ng/µl) overnight at 37^{o}C as described [88].

Following overnight digestion, the supernatant was transferred to a fresh tube and the tryptic peptides from the gel pieces were extracted twice with 50% acetonitrile/2% formic acid and combined with the supernatants. The tryptic peptides were vacuum centrifuged to remove acetonitrile and desalted on a pre-equilibrated C18 Omix tip. The eluted peptides were further dried under vacuum centrifugation. The peptide pellet was the resuspended in 12uL of 0.1% formic acid and 10 µl was loaded for LC-MS/MS analysis.

Tryptic peptides were separated using an UHPLC Dionex Ultimate 3000 RSLC nano (ThermoFisher, USA) equipped with a Thermo Acclaim™ PepMap™ 100 C18 column (75 µm diameter, 3 µm particle size, 150 mm length) employing a 60 min gradient (2%–26% v/v acetonitrile, 0.1% v/v formic acid for 40 mins followed by 50% v/v acetonitrile, 0.1% v/v formic acid for 10 mins and 80% v/v acetonitrile, 0.1% v/v formic acid for 8 mins) with a flow rate of 300 nl/min. The peptides were eluted and ionized into Q-Exactive Plus mass spectrometer (ThermoFisher, USA). The electrospray source was fitted with an emitter tip 10µm (ThermoFisher, USA) and maintained at 1.6 kV electrospray voltage. FTMS analysis was carried out with a 70,000 resolution and an AGC target of $1x10^{6}$ ions in full MS (m/z range 400-2000); and MS/MS scans were carried out at 17,500 resolution with an AGC target of $2x10^{4}$ ions. Maximum injection times were set to 30 and 50 milliseconds respectively. A top-10 method was employed for MS/MS selection, ion selection threshold for triggering MS/MS fragmentation was set to $1x10^{4}$ counts, isolation width of 2.0 Da, and dynamic exclusion for 20 seconds was used to perform HCD fragmentation with normalized collision energy of 27.

Raw spectra files were processed using the Proteome Discoverer 2.4 software (Thermo) against the Swissprot database (organism *Homo sapiens*, version 25/10/2017 with 42252 sequences) incorporating the Sequest search algorithm. Peptide identifications were determined using a 20-ppm precursor ion tolerance and a 0.1 Da MS/MS fragment ion

tolerance for FTMS and HCD fragmentation. Carbamidomethylation modification of cysteines was considered a static modification while oxidation of methionine, and acetyl modification on N-terminal residues were set as variable modifications allowing for maximum two missed cleavages. The data was processed through Percolator for estimation of false discovery rates. Protein identifications were validated employing a q-value of 0.01.

Data analysis

Data analysis was performed using GraphPad Prism (8) software. Group comparisons were made using one-way ANOVA tests, followed by a Tukey post-hoc to identify differences. Where data did not meet assumptions for one-way ANOVA, a non-parametric test, Kruskal Wallis, was used. Co-treatment studies were analyzed using a two-way ANOVA (Factor 1: treatment with sodium butyrate, Factor 2: treatment with autophagy inhibitor, bafilomycin 1A/chloroquine). Flow cytometry experiments were also analyzed using a two-way ANOVA to examine the effect of drug treatments on insoluble particle size (Factor 1: drug treatment, Factor 2: insoluble particle size). Co-treatment data was analyzed for main effects and interaction effects. Post-hoc multiple comparisons were used to determine statistical significance between treatment groups. Comparison between two different groups was analyzed using student t-tests. All results presented are mean ± standard error mean (SEM) with statistical significance which is defined as $p \leq 0.05$.

Acknowledgements

The authors would like to thank Henry Paulson for the MJD antibody and EGFP-ATXN3 plasmids. We also thank staff members (past and present) of the zebrafish facility at Macquarie University for the care of the zebrafish described within this manuscript. The authors would also like to acknowledge Dr Elena Shklovskaya and Miss Bernadette Pederson for providing technical support and analysis advice for flow cytometry experiments.

Funding

This work was funded by: MJD Foundation, Australia; Australian National Health and Medical Research Council (Project Grant 1069235); The Snow Foundation, Australia; Macquarie University DVCR Start-up Funding and Research Development Grant. The Swedish SCA Network also provided donation support for this work.

Disclosure statement

The authors declare that they have no conflict of interests.

Figure Legends

Figure 1. SH-SY5Y cell culture modelling revealed the presence of ataxin-3 aggregates

(A-C) Stably transfected SH-SY5Y cells were confirmed to express human ataxin-3 after immunostaining for ataxin-3. (A) Cells expressing an empty vector control did not display aggregated ataxin-3, however cells expressing either (B) human ataxin-3 with 28 polyQ repeats, or (C) ataxin-3 with 84 polyQ repeats displayed ataxin-3 positive aggregates (indicated by white arrows, scale bar: 20 µm). (D) In SH-SY5Y cells that stably expressed human ataxin-3-84Q, ataxin-3 positive aggregates were found to colocalise with ubiquitin (scale bar: 10 µm). (E) Quantification of the number of aggregates present revealed that ataxin-3 84Q cells possessed a higher number of aggregates compared to ataxin-3 28Q and the vector control (***$p<0.001$ and ****$p<0.0001$ respectively, n=19-24). (F) Flow cytometric analysis confirmed that EGFP-tagged polyglutamine expanded ataxin-3 harboured more GFP^+ particles compared to the vector control (**$p<0.01$, n=4-7). (G) Analysis of the mean diameter of the GFP^+ particles between the genotypes found that the MJD cells had larger GFP^+ particles compared to the vector control (*$p<0.05$, n=5-12). (H) Immunoblotting SH-SY5Y cells with ataxin-3 confirmed expression of human ataxin-3 28Q and 84Q as well as endogenous ataxin-3. An additional band above the 84Q monomeric band was found, suggesting an ataxin-3 oligomer. (I) Quantification of human ataxin-3 monomers indicated increased ataxin-3 levels in ataxin-3 28Q and 84Q compared to the vector control ***($p<0.001$ and ****$p<0.001$ respectively; n=6), and (J) Quantification of ataxin-3 dimers revealed that more dimer was present in the Ataxin-3 84Q cells compared to the other genotypes (****$p<0.0001$; n=6). Results are shown as mean ± SEM. Statistical analysis was performed using a one-way ANOVA followed by a Tukey's post hoc test.

Figure 2. Transgenic zebrafish modelling MJD have histone hypoacetylation.

(A) Western blot analysis showed that protein lysates of 6-day-old transgenic MJD zebrafish expressing human ataxin-3 (23Q and 84Q) had full-length (FL), ataxin-3 cleavage fragments (CF) and endogenous ataxin-3 (ZF). When probed for acetylated histone 3 at lysine 9 (H3K9) and acetylated histone 4 at lysine 5 (H4K5), there was a polyQ-dependent decrease in these acetylated histones. (B) Quantification of the acetylated histone 3 and (C) acetylated histone 4 showed a reduction with polyQ expanded ataxin-3 compared to the non-transgenic control (p*<0.05; n=3-5). Results are mean ± SEM. Statistical analysis was performed using a non-parametric one-way ANOVA (Kruskal Wallis) test.

Figure 3: Treatment with sodium butyrate increases histone acetylation and affects ataxin-3 proteinopathy in MJD SH-SY5Y cells.

(A) Western blots of SH-SY5Y stably expressing ataxin-3-84Q cells treated with 3 mM SB or vehicle control (autoclaved water) were probed for acetylated histone 3 (H3K9) and acetylated histone 4 (H4K5). (B) Densitometry of acetylated H3K9 and (C) H4K5 revealed an increase with SB treatment compared to vehicle control (**$p<0.01$, n=6). (D) Immunostaining for ataxin-3 revealed a reduction in the amount of ataxin-3 positive aggregates after treatment with SB, compared to vehicle treatment (white arrows). (E) Quantification of the number of ataxin-3 positive aggregates revealed decreased aggregates in SB-treated ataxin-3 84Q cells

compared to the vehicle treated control (*p<0.05, n=6). (F) SB treatment also reduced the average size of the GFP^+ particles following flow cytometric analysis (***p<0.001, n=7). (G) Western blot of SH-SY5Y stably expressing Ataxin-3-84Q cells treated with 3 mM SB or vehicle were probed for ataxin-3. (H) Densitometry of ataxin-3 dimers indicated that decreased dimers were present following treatment with SB compared to vehicle control (*p<0.05, n=6). Data represents mean ± SEM. The statistical analysis was performed by an unpaired student t-test.

Figure 4. Sodium butyrate treatment rectifies histone hypoacetylation and rescues the motor phenotype in MJD zebrafish.
Zebrafish expressing ataxin-3-84Q were treated with 250 µM, 500 µM or 1 mM sodium butyrate (SB), or vehicle control, between 1-6 days post fertilization (dpf). (A) Protein lysates of the 6dpf zebrafish treated either SB or the vehicle control underwent western blotting and checked for ataxin-3, acetylated histone 3 (H3K9) and acetylated histone 4 (H4K5). (B) Quantification of acetylated histone 3 revealed a dose-dependent increase of acetylated H3K9 following SB treatment (500 µM, *p<0.05; 1 mM, **p<0.01, n=3-9), whilst (C) quantification of acetylated H4K5 revealed 1 mM SB was only able to significantly rectify hypoacetylation compared to the vehicle control (**p<0.01, n=3-10). (D) Swimming trajectories of 6dpf zebrafish after treatment with vehicle versus 1 mM SB treatment (Green, slow movement; red, fast movement). (E) Motor behaviour analysis showed vehicle treated ataxin-3-84Q zebrafish swam shorter distances compared to the non-transgenic controls (**p<0.01) whilst 6dpf ataxin-3-84Q larvae treated with 1 mM SB ameliorated the motor dysfunction (**p<0.01, n=64-158). Data represents mean ± SEM. Statistical analysis was performed by a non-parametric one-way ANOVA (Kruskal Wallis) test.

Figure 5: Treatment with sodium butyrate induces autophagy and decreases large-sized protein aggregates in MJD SH-SY5Y cells.
(A) Immunofluorescent staining of SH-SY5Y cells stably expressing ataxin-3 84Q after treatment in 3 mM SB alone for 72 hours and/or 100 nM bafilomycin A1 for 2 hours bafilomycin compared to a vehicle treatment. Cells were stained with ataxin-3 or LC3B (Scale bar: 10 µm). (B) Two way ANOVA revealed that SB treatment had decreased the number of large aggregates (p<0.01), however bafilomycin cotreatment had no effect on aggregates numbers (n=3-4). C) Western blot analysis was performed on lysates of SH-SY5Y cells stably expressing ataxin-3 84Q following treatment with 3 mM SB for 72 hours. The blots were probed for ataxin-3, LC3B and p62. (D) Densitometry analysis of LC3B showed increased LC3BII/LC3BI ratio in SB and bafilomycin A1 co-treated cells when compared to vehicle treatment (***p<0.001), SB treatment (***p<0.001) and bafilomycin A1 treatment alone (**p<0.01). (E) Western blotting also revealed an SB-dependent decrease in p62 levels, with SB induced decreased p62 when compared to vehicle treatment (*p<0.05) and bafilomycin A1 treatment (***p<0.001). Co-treatment with SB and bafilomycin A1 also produced a decrease in p62 when compared to bafilomycin alone (*p<0.05). (F) Densitometry of ataxin-3 dimer bands indicated a decrease in the amount of dimer present in SB treated cells compared to vehicle treated cells (*p<0.05, n=7). A decrease in the amount of ataxin-3 dimer is also evident in the SB and bafilomycin A1 cotreated cells. Data represents mean ± SEM. The statistical analysis was performed using a two-way ANOVA followed with Tukey post hoc test.

Figure 6: Sodium butyrate treatment on human ataxin-3 expressing SH-SY5Y cells induce autophagy and affect ataxin-3 aggregation status.
(A) Flow cytometric scatter plots of transiently expressing EGFP-fused ataxin-3 84Q SH-SY5Y cells treated with 3mM sodium butyrate (SB) for 24 hours and/or the autophagy inhibitor 100 nM bafilomycin A1 (BafA1) for 2 hours. Dotted lines represent a particle size diameter of 6 µm. (B) Quantification of the number of Triton-X insoluble GFP^{+} particles revealed that the number of particles had increased with SB treatment compared to the vehicle treatment and BafA1 alone (****p<0.0001). SB/BafA1 co-treatment also had a higher number of Triton-X insoluble $GFP^{\pm}$ particles compared to BafA1 treatment alone and vehicle treatment (**p<0.01, n=3). (C) Analysis of aggregate size (mean diameter) revealed a significant reduction in aggregate size following SB treatment and SB/BafA1 co-treatment compared to the vehicle treated ataxin-3 84Q cells (*p<0.05, n=3). Data represents mean ± SEM. Statistical analysis performed was a two-way ANOVA followed by Tukey post-hoc test.

Figure 7. Removal of ataxin-3 dimers by sodium butyrate is mediated by autophagy.
(A) Western blots were performed of SH-SY5Y cells stably expressing ataxin-3 84Q treated with sodium butyrate (SB, 3 mM) and/or 3MA (5 mM) for 72 hrs and probed for ataxin-3. (B) Quantification of ataxin-3 dimers indicated that SB-treatment had induced a reduction in the amount of dimerised ataxin-3, compared to vehicle treatment (**p<0.01), and addition of 3MA treatment prevented the removal of the ataxin-3 dimers (**p<0.01, n=6). Data represents mean ± SEM. Statistical analysis performed was a two-way ANOVA followed by a Tukey post-hoc analysis.

Figure 8: Treatment with sodium butyrate induces autophagy in MJD zebrafish model producing beneficial effects on zebrafish swimming.
(A) Western blots were performed on protein lysates from ataxin-3-84Q zebrafish larvae treated with either 1 mM sodium butyrate (SB) alone, 1.5 mM chloroquine (Chlor) alone or co-treatment of SB and Chlor, between 1-6 days post fertilization (dpf). The immunoblots were probed for ataxin-3 and LC3B levels. (B) Quantification of LC3B levels after treatment with 1mM SB, 1.5 mM Chlor and 3 mM Chlor found a dose dependent increase in LC3II levels with chloroquine compared to the vehicle control (1.5 mM, ***p<0.001 and 3 mM, ****p<0.0001). However, 3 mM Chlor co-treatment with SB increased LC3II levels compared to 3mM Chlor alone (*p<0.05, n=4-15). (C) Swimming trajectories of zebrafish treated with either vehicle control, 1 mM SB or SB/1.5 mM chloroquine show that SB increases the amount of fast swimming and SB/Chlor co-treatment decreases this (green, slow movement; red, fast movement). (D) Quantification of the total distance swum by each animal demonstrates that SB treatment rescues the motor impairment seen in vehicle treated ataxin-3 84Q zebrafish (****p<0.0001) and those receiving 1.5 mM chloroquine or SB/chloroquine co-treatment (****p<0.0001, n=81-256). Data represents mean ± SEM. Statistical analysis was performed using a two-way ANOVA followed by a Tukey post-hoc test.

Figure 9. Treating wild-type mice with sodium butyrate can produce autophagy induction in the brain.
Figure 8. (A) Schematic of the SB treatment regime for wild-type mice, including three days of intraperitoneal administration of 200 mg/kg SB, or vehicle, followed by euthanasia and extraction of the brain 60 minutes after the third injection. (B) Western blotting of protein lysates from the brains of the wild-type mice following treatment with either vehicle or SB revealed an increase in LC3B levels. (C) Densitometric analysis confirmed that there was a significant increase in LC3B levels following SB treatment compared to treatment with the vehicle control (*$p<0.05$, n=3-4). Data represents mean ± SEM. Statistical analysis was performed using a non-parametric student t-test.

Supplementary 1: Ataxin-3 expressing SH-SY5Y cells reveals increased aggregates in polyglutamine expanded ataxin-3 cells.
(A) Representative scatter plots of SH-SY5Y cells transiently expressing EGFP-tagged ataxin-3 28Q or 84Q, as well as EGFP empty vector and untransfected controls, after flow cytometric analysis in the presence of 0.5% Triton-X 100. Top panel represents the number of nuclei detected after cells were stained with DAPI. Bottom panel represents the number and size of GFP^+ particles. (B) Quantifying the number of Triton-X insoluble GFP^+ particles showed EGFP-ataxin-3 84Q cells possessed more particles compared to the empty vector control (*$p<0.05$, n=4-8). Data represents mean ± SEM. Statistical analysis performed was a one-way ANOVA followed by Tukey post-hoc test.

Supplementary 2. Validation of ataxin-3 dimers expressed in ataxin-3-84Q SH-SY5Y cells using mass spectrometry.
Representative western blot detecting the total protein found in SH-SY5Y cells stably expressing ataxin-3 84Q. White dotted lines define the different fractions based on protein size.

Supplementary Table 1. Identified ataxin-3 peptides in ataxin-3-84Q SH-SY5Y cells using mass spectrometry.

Protein lysates of SH-SY5Y cells expressing ataxin-3-84Q were subjected to SDS-PAGE and different fractions were separated by size and subjected to using mass spectrometry aiming to identify ataxin-3 dimers. Mass spectrometry identified ataxin-3 protein within Fraction 2, which contained proteins of between 120-200 kDa in size, where we predicted to find ataxin-3 dimers.

Supplementary 3: SH-SY5Y cells expressing ataxin-3 present with histone hypoacetylation.

(A) Western blot of stably expressing ataxin-3 28Q and 84Q SH-SY5Y cells comparing levels of ataxin-3, acetylated histone 3 at lysine 9 (H3K9) and acetylated histone 4 at lysine 5 (H4K5). (B) Densitometric analysis of H3K9 revealed an increase in H3K9 levels in ataxin-3 28Q cells compared to the vehicle control (*$p<0.05$), whilst ataxin-3 84Q cells had

decreased H3K9 levels compared to the ataxin-3 28Q cells (*p<0.05, n=5). (C) Quantifying the levels of H4K5 were found to be similar between the different genotypes. Data represents mean ± SEM. Statistical analysis performed was a non-parametric one-way ANOVA, followed by Kruskal Wallis test.

Supplementary 4: High concentrations of the drug chloroquine affect motor behaviour in non-transgenic zebrafish.

(A) Treatment of non-transgenic zebrafish embryos with either vehicle control, 1.5 mM or 3 mM chloroquine (chlor) between 1-6 days post fertilization (dpf) revealed that 3 mM chloroquine affects zebrafish locomotion compared to both vehicle treatment and 1.5 mM chlor (**p<0.01, n=32-39). Treatment with 1.5 mM chlor did not affect the movement compared to vehicle control treatment (p=0.993). Data represents mean ± SEM. Statistical analysis performed was a one-way ANOVA followed by a Tukey post-hoc test.

References

1. Costa, M.d.C. and H.L. Paulson, *Toward understanding Machado-Joseph disease.* Progress in neurobiology, 2012. **97**(2): p. 239-257.
2. Rüb, U., et al., *Clinical features, neurogenetics and neuropathology of the polyglutamine spinocerebellar ataxias type 1, 2, 3, 6 and 7.* Prog Neurobiol, 2013. **104**: p. 38-66.
3. Privett, B.K. and R.H. Kardon, *Spinocerebellar Ataxia with Ophthalmoplegia: 46-y.o. male presenting with progressive esotropia.* 2010.
4. Durr, A., et al., *Spinocerebellar ataxia 3 and Machado-Joseph disease: clinical, molecular, and neuropathological features.* Ann Neurol, 1996. **39**(4): p. 490-9.
5. Ranum, L.P., et al., *Spinocerebellar ataxia type 1 and Machado-Joseph disease: incidence of CAG expansions among adult-onset ataxia patients from 311 families with dominant, recessive, or sporadic ataxia.* American journal of human genetics, 1995. **57**(3): p. 603-608.
6. Schols, L., et al., *Trinucleotide expansion within the MJD1 gene presents clinically as spinocerebellar ataxia and occurs most frequently in German SCA patients.* Hum Mol Genet, 1995. **4**(6): p. 1001-5.
7. Bettencourt, C., et al., *The (CAG)n tract of Machado-Joseph Disease gene (ATXN3): a comparison between DNA and mRNA in patients and controls.* European journal of human genetics : EJHG, 2010. **18**(5): p. 621-623.
8. Burt, T., et al., *Machado-Joseph disease in east Arnhem Land, Australia: chromosome 14q32.1 expanded repeat confirmed in four families.* Neurology, 1996. **46**(4): p. 1118-22.
9. Kawaguchi, Y., et al., *CAG expansions in a novel gene for Machado-Joseph disease at chromosome 14q32.1.* Nat Genet, 1994. **8**(3): p. 221-8.
10. Takiyama, Y., et al., *The gene for Machado-Joseph disease maps to human chromosome 14q.* Nat Genet, 1993. **4**(3): p. 300-4.
11. Nascimento-Ferreira, I., et al., *Beclin 1 mitigates motor and neuropathological deficits in genetic mouse models of Machado-Joseph disease.* Brain, 2013. **136**(Pt 7): p. 2173-88.
12. Maciel, P., et al., *Correlation between CAG repeat length and clinical features in Machado-Joseph disease.* Am J Hum Genet, 1995. **57**(1): p. 54-61.
13. Matsumura, R., et al., *Relationship of (CAG)nC configuration to repeat instability of the Machado-Joseph disease gene.* Hum Genet, 1996. **98**(6): p. 643-5.
14. Schmidt, T., et al., *An isoform of ataxin-3 accumulates in the nucleus of neuronal cells in affected brain regions of SCA3 patients.* Brain Pathol, 1998. **8**(4): p. 669-79.
15. Yamada, M., S. Tsuji, and H. Takahashi, *Pathology of CAG repeat diseases.* Neuropathology, 2000. **20**(4): p. 319-25.
16. Goti, D., et al., *A mutant ataxin-3 putative-cleavage fragment in brains of Machado-Joseph disease patients and transgenic mice is cytotoxic above a critical concentration.* J Neurosci, 2004. **24**(45): p. 10266-79.
17. Evert, B.O., et al., *Ataxin-3 represses transcription via chromatin binding, interaction with histone deacetylase 3, and histone deacetylation.* J Neurosci, 2006. **26**(44): p. 11474-86.
18. Evers, M.M., L.J.A. Toonen, and W.M.C. van Roon-Mom, *Ataxin-3 protein and RNA toxicity in spinocerebellar ataxia type 3: current insights and emerging therapeutic strategies.* Molecular neurobiology, 2014. **49**(3): p. 1513-1531.

19. Li, F., et al., *Ataxin-3 is a histone-binding protein with two independent transcriptional corepressor activities.* J Biol Chem, 2002. **277**(47): p. 45004-12.
20. Jung, J. and N. Bonini, *CREB-Binding Protein Modulates Repeat Instability in a Drosophila Model for PolyQ Disease.* Science, 2007. **315**(5820): p. 1857-1859.
21. Chou, A.-H., et al., *Polyglutamine-expanded ataxin-3 impairs long-term depression in Purkinje neurons of SCA3 transgenic mouse by inhibiting HAT and impairing histone acetylation.* Brain Research, 2014. **1583**: p. 220-229.
22. Minamiyama, M., et al., *Sodium butyrate ameliorates phenotypic expression in a transgenic mouse model of spinal and bulbar muscular atrophy.* Hum Mol Genet, 2004. **13**(11): p. 1183-92.
23. Yi, J., et al., *Sodium valproate alleviates neurodegeneration in SCA3/MJD via suppressing apoptosis and rescuing the hypoacetylation levels of histone H3 and H4.* PloS one, 2013. **8**(1): p. e54792-e54792.
24. Chou, A.-H., et al., *HDAC inhibitor sodium butyrate reverses transcriptional downregulation and ameliorates ataxic symptoms in a transgenic mouse model of SCA3.* Neurobiology of Disease, 2011. **41**(2): p. 481-488.
25. Haggarty, S.J. and L.H. Tsai, *Probing the role of HDACs and mechanisms of chromatin-mediated neuroplasticity.* Neurobiol Learn Mem, 2011. **96**(1): p. 41-52.
26. Liu, H., et al., *Butyrate: A Double-Edged Sword for Health?* Adv Nutr, 2018. **9**(1): p. 21-29.
27. Wu, Y.-L., et al., *Treatment with Caffeic Acid and Resveratrol Alleviates Oxidative Stress Induced Neurotoxicity in Cell and Drosophila Models of Spinocerebellar Ataxia Type3.* Scientific Reports, 2017. **7**(1): p. 11641.
28. Graff, J., et al., *An epigenetic blockade of cognitive functions in the neurodegenerating brain.* Nature, 2012. **483**(7388): p. 222-6.
29. Hockly, E., et al., *Suberoylanilide hydroxamic acid, a histone deacetylase inhibitor, ameliorates motor deficits in a mouse model of Huntington's disease.* Proc Natl Acad Sci U S A, 2003. **100**(4): p. 2041-6.
30. Kazantsev, A.G. and L.M. Thompson, *Therapeutic application of histone deacetylase inhibitors for central nervous system disorders.* Nat Rev Drug Discov, 2008. **7**(10): p. 854-68.
31. Krainc, D., *Clearance of mutant proteins as a therapeutic target in neurodegenerative diseases.* Arch Neurol, 2010. **67**(4): p. 388-92.
32. Richon, V.M., et al., *A class of hybrid polar inducers of transformed cell differentiation inhibits histone deacetylases.* Proc Natl Acad Sci U S A, 1998. **95**(6): p. 3003-7.
33. Vigushin, D.M., et al., *Trichostatin A Is a Histone Deacetylase Inhibitor with Potent Antitumor Activity against Breast Cancer in Vivo.* Clinical Cancer Research, 2001. **7**(4): p. 971-976.
34. Yeung, F., et al., *Modulation of NF-κB-dependent transcription and cell survival by the SIRT1 deacetylase.* The EMBO Journal, 2004. **23**(12): p. 2369-2380.
35. Göttlicher, M., et al., *Valproic acid defines a novel class of HDAC inhibitors inducing differentiation of transformed cells.* The EMBO journal, 2001. **20**(24): p. 6969-6978.
36. Sealy, L. and R. Chalkley, *The effect of sodium butyrate on histone modification.* Cell, 1978. **14**(1): p. 115-21.

37. Canani, R.B., et al., *Potential beneficial effects of butyrate in intestinal and extraintestinal diseases.* World J Gastroenterol, 2011. **17**(12): p. 1519-28.
38. Ferrante, R.J., et al., *Histone deacetylase inhibition by sodium butyrate chemotherapy ameliorates the neurodegenerative phenotype in Huntington's disease mice.* J Neurosci, 2003. **23**(28): p. 9418-27.
39. Whiten, D.R., et al., *Rapid flow cytometric measurement of protein inclusions and nuclear trafficking.* Scientific Reports, 2016. **6**(1): p. 31138.
40. Watchon, M., et al., *Calpain Inhibition Is Protective in Machado–Joseph Disease Zebrafish Due to Induction of Autophagy.* The Journal of Neuroscience, 2017. **37**(32): p. 7782-7794.
41. Klionsky, D.J., et al., *Guidelines for the use and interpretation of assays for monitoring autophagy (3rd edition).* Autophagy, 2016. **12**(1): p. 1-222.
42. Santana, M.M., et al., *Trehalose alleviates the phenotype of Machado–Joseph disease mouse models.* Journal of Translational Medicine, 2020. **18**(1): p. 161.
43. Yoshizawa, T., H. Yoshida, and S.i. Shoji, *Differential susceptibility of cultured cell lines to aggregate formation and cell death produced by the truncated Machado-Joseph disease gene product with an expanded polyglutamine stretch.* Brain Research Bulletin, 2001. **56**(3): p. 349-352.
44. Paulson, H.L., et al., *Intranuclear inclusions of expanded polyglutamine protein in spinocerebellar ataxia type 3.* Neuron, 1997. **19**(2): p. 333-44.
45. Rüb, U., E.R. Brunt, and T. Deller, *New insights into the pathoanatomy of spinocerebellar ataxia type 3 (Machado–Joseph disease).* Current Opinion in Neurology, 2008. **21**(2): p. 111-116.
46. Weishäupl, D., et al., *Physiological and pathophysiological characteristics of ataxin-3 isoforms.* Journal of Biological Chemistry, 2018.
47. Yu, W.H., et al., *Metabolic activity determines efficacy of macroautophagic clearance of pathological oligomeric alpha-synuclein.* Am J Pathol, 2009. **175**(2): p. 736-47.
48. Jana, M.K., et al., *Membrane-bound tetramer and trimer Aβ oligomeric species correlate with toxicity towards cultured neurons.* Journal of Neurochemistry, 2016. **136**(3): p. 594-608.
49. Kim, H.J., et al., *Selective neuronal degeneration induced by soluble oligomeric amyloid beta protein.* Faseb j, 2003. **17**(1): p. 118-20.
50. Lajoie, P. and E.L. Snapp, *Formation and toxicity of soluble polyglutamine oligomers in living cells.* PloS one, 2010. **5**(12): p. e15245-e15245.
51. Outeiro, T.F., et al., *Formation of toxic oligomeric alpha-synuclein species in living cells.* PloS one, 2008. **3**(4): p. e1867-e1867.
52. Sánchez, I., C. Mahlke, and J. Yuan, *Pivotal role of oligomerization in expanded polyglutamine neurodegenerative disorders.* Nature, 2003. **421**(6921): p. 373-379.
53. Zhang, Y., et al., *Anesthetic propofol attenuates the isoflurane-induced caspase-3 activation and Aβ oligomerization.* PLoS One, 2011. **6**(11): p. e27019.
54. La Vitola, P., et al., *Cellular prion protein neither binds to alpha-synuclein oligomers nor mediates their detrimental effects.* Brain, 2019. **142**(2): p. 249-254.
55. Kim, Y.E., et al., *Soluble Oligomers of PolyQ-Expanded Huntingtin Target a Multiplicity of Key Cellular Factors.* Mol Cell, 2016. **63**(6): p. 951-64.

56. Haass, C. and D.J. Selkoe, *Soluble protein oligomers in neurodegeneration: lessons from the Alzheimer's amyloid beta-peptide.* Nat Rev Mol Cell Biol, 2007. **8**(2): p. 101-12.
57. Walsh, D.M. and D.J. Selkoe, *Oligomers on the brain: the emerging role of soluble protein aggregates in neurodegeneration.* Protein Pept Lett, 2004. **11**(3): p. 213-28.
58. Menzies, F.M., et al., *Autophagy induction reduces mutant ataxin-3 levels and toxicity in a mouse model of spinocerebellar ataxia type 3.* Brain, 2010. **133**(Pt 1): p. 93-104.
59. Cunha-Santos, J., et al., *Caloric restriction blocks neuropathology and motor deficits in Machado-Joseph disease mouse models through SIRT1 pathway.* Nature communications, 2016. **7**: p. 11445-11445.
60. Qin, Z.-H., et al., *Huntingtin Bodies Sequester Vesicle-Associated Proteins by a Polyproline-Dependent Interaction.* The Journal of Neuroscience, 2004. **24**(1): p. 269-281.
61. Ravikumar, B., et al., *Inhibition of mTOR induces autophagy and reduces toxicity of polyglutamine expansions in fly and mouse models of Huntington disease.* Nature Genetics, 2004. **36**(6): p. 585-595.
62. Sasazawa, Y., et al., *Conophylline protects cells in cellular models of neurodegenerative diseases by inducing mammalian target of rapamycin (mTOR)-independent autophagy.* J Biol Chem, 2015. **290**(10): p. 6168-78.
63. Martín-Aparicio, E., et al., *Proteasomal-Dependent Aggregate Reversal and Absence of Cell Death in a Conditional Mouse Model of Huntington's Disease.* The Journal of Neuroscience, 2001. **21**(22): p. 8772-8781.
64. Williams, A., et al., *Novel targets for Huntington's disease in an mTOR-independent autophagy pathway.* Nat Chem Biol, 2008. **4**(5): p. 295-305.
65. Sarkar, S., et al., *Small molecules enhance autophagy and reduce toxicity in Huntington's disease models.* Nature Chemical Biology, 2007. **3**(6): p. 331-338.
66. Perera, N.D., et al., *Rilmenidine promotes MTOR-independent autophagy in the mutant SOD1 mouse model of amyotrophic lateral sclerosis without slowing disease progression.* Autophagy, 2018. **14**(3): p. 534-551.
67. Duncan, C., T. Papanikolaou, and L.M. Ellerby, *Autophagy: PolyQ toxic fragment turnover.* Autophagy, 2010. **6**(2): p. 312-314.
68. Yamamoto , A., M.L. Cremona , and J.E. Rothman *Autophagy-mediated clearance of huntingtin aggregates triggered by the insulin-signaling pathway.* Journal of Cell Biology, 2006. **172**(5): p. 719-731.
69. Watanabe, Y., et al., *p62/SQSTM1-Dependent Autophagy of Lewy Body-Like α-Synuclein Inclusions.* PLOS ONE, 2013. **7**(12): p. e52868.
70. Qiao, C.M., et al., *Sodium butyrate causes alpha-synuclein degradation by an Atg5-dependent and PI3K/Akt/mTOR-related autophagy pathway.* Exp Cell Res, 2019: p. 111772.
71. Simões, A.T., et al., *Calpain inhibition reduces ataxin-3 cleavage alleviating neuropathology and motor impairments in mouse models of Machado-Joseph disease.* Hum Mol Genet, 2014. **23**(18): p. 4932-44.
72. Todd, T.W. and J. Lim, *Aggregation formation in the polyglutamine diseases: protection at a cost?* Mol Cells, 2013. **36**(3): p. 185-94.
73. Takahashi, T., S. Katada, and O. Onodera, *Polyglutamine diseases: where does toxicity come from? what is toxicity? where are we going?* J Mol Cell Biol, 2010. **2**(4): p. 180-91.

74. Holmes, W.M., C.L. Klaips, and T.R. Serio, *Defining the limits: Protein aggregation and toxicity in vivo.* Crit Rev Biochem Mol Biol, 2014. **49**(4): p. 294-303.
75. Zhang, Y., et al., *A new role for oxidative stress in aging: The accelerated aging phenotype in Sod1−/− mice is correlated to increased cellular senescence.* Redox Biology, 2017. **11**: p. 30-37.
76. Chou, A.-H., et al., *Polyglutamine-expanded ataxin-3 causes cerebellar dysfunction of SCA3 transgenic mice by inducing transcriptional dysregulation.* Neurobiology of Disease, 2008. **31**(1): p. 89-101.
77. Chuang, D.M., et al., *Multiple roles of HDAC inhibition in neurodegenerative conditions.* Trends Neurosci, 2009. **32**(11): p. 591-601.
78. Chen, P.S., et al., *Valproate protects dopaminergic neurons in midbrain neuron/glia cultures by stimulating the release of neurotrophic factors from astrocytes.* Molecular Psychiatry, 2006. **11**(12): p. 1116-1125.
79. Leng, Y. and D.-M. Chuang, *Endogenous α-Synuclein Is Induced by Valproic Acid through Histone Deacetylase Inhibition and Participates in Neuroprotection against Glutamate-Induced Excitotoxicity.* The Journal of Neuroscience, 2006. **26**(28): p. 7502-7512.
80. Vidoni, C., et al., *Resveratrol protects neuronal-like cells expressing mutant Huntingtin from dopamine toxicity by rescuing ATG4-mediated autophagosome formation.* Neurochem Int, 2018. **117**: p. 174-187.
81. Morselli, E., et al., *Spermidine and resveratrol induce autophagy by distinct pathways converging on the acetylproteome.* The Journal of cell biology, 2011. **192**(4): p. 615-629.
82. Zhang, Y., et al., *Valproic acid protects against MPP(+)-mediated neurotoxicity in SH-SY5Y Cells through autophagy.* Neurosci Lett, 2017. **638**: p. 60-68.
83. Wang, X., et al., *Valproate Attenuates 25-kDa C-Terminal Fragment of TDP-43-Induced Neuronal Toxicity via Suppressing Endoplasmic Reticulum Stress and Activating Autophagy.* Int J Biol Sci, 2015. **11**(7): p. 752-61.
84. Li, X.Z., et al., *Therapeutic effects of valproate combined with lithium carbonate on MPTP-induced parkinsonism in mice: possible mediation through enhanced autophagy.* Int J Neurosci, 2013. **123**(2): p. 73-9.
85. Park, H.C., et al., *Analysis of upstream elements in the HuC promoter leads to the establishment of transgenic zebrafish with fluorescent neurons.* Dev Biol, 2000. **227**(2): p. 279-93.
86. Cunliffe, V.T., *Zebrafish: A Practical Approach. Edited by C. NÜSSLEIN-VOLHARD and R. DAHM. Oxford University Press. 2002. 322 pages. ISBN 0 19 963808 X. Price £40.00 (paperback). ISBN 0 19 963809 8. Price £80.00 (hardback).* Genetical Research, 2003. **82**(1): p. 79-79.
87. Schindelin, J., et al., *Fiji: an open-source platform for biological-image analysis.* Nature Methods, 2012. **9**(7): p. 676-682.
88. Lee, A., et al., *Rat liver membrane glycoproteome: enrichment by phase partitioning and glycoprotein capture.* J Proteome Res, 2009. **8**(2): p. 770-81.

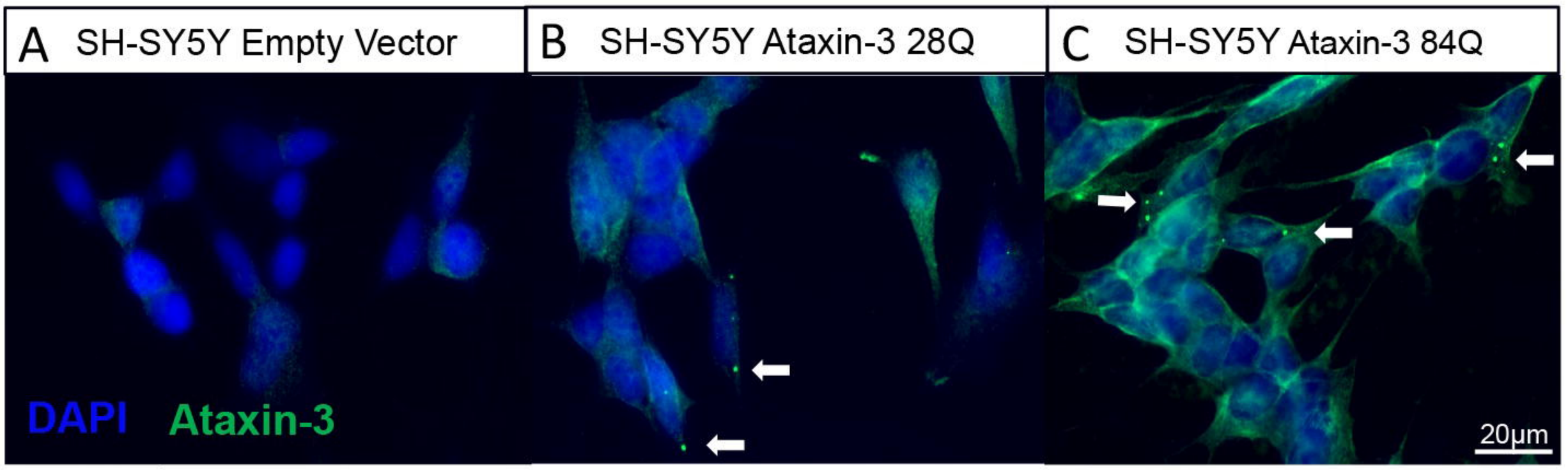

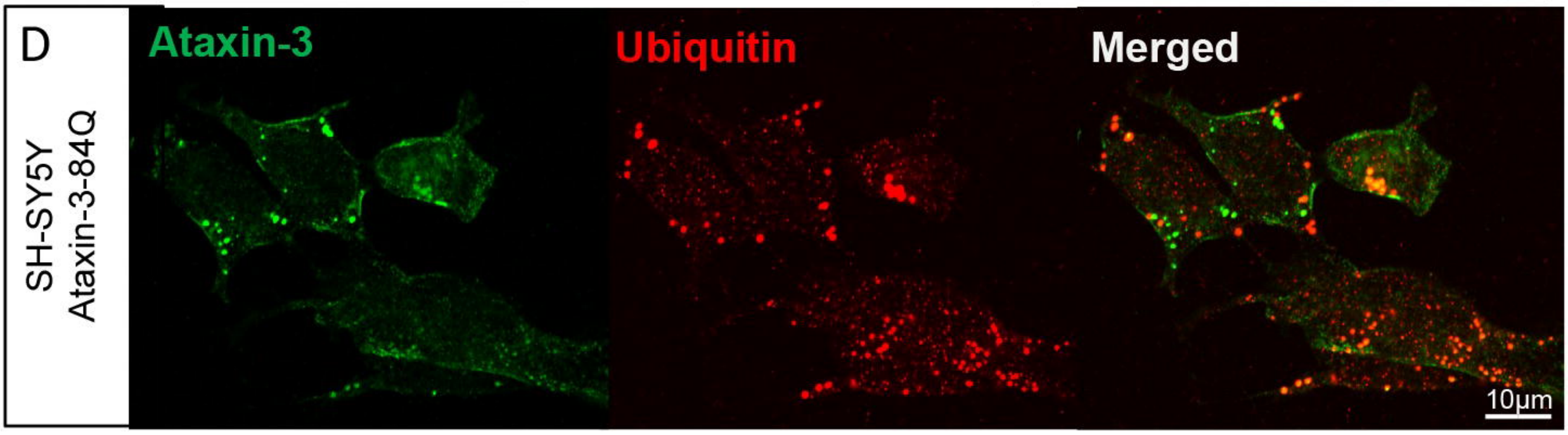

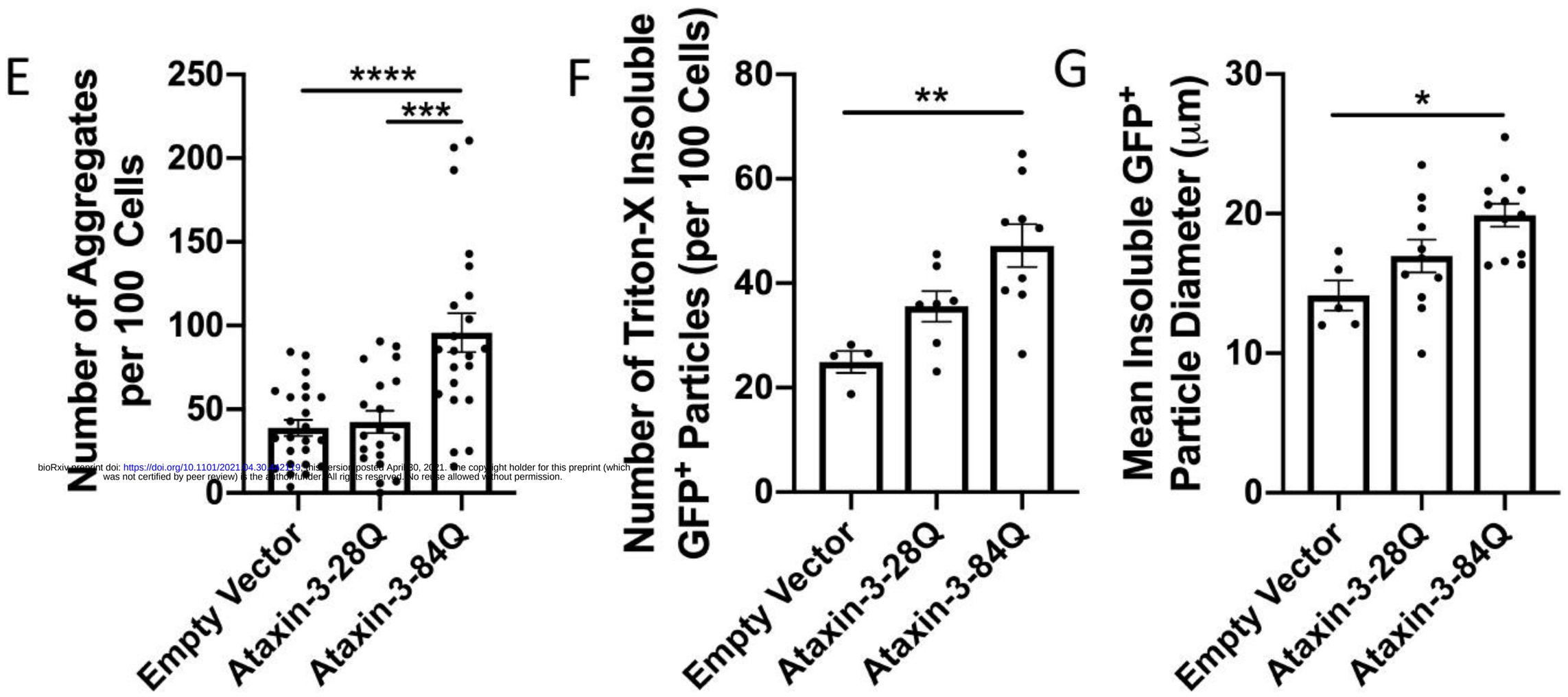

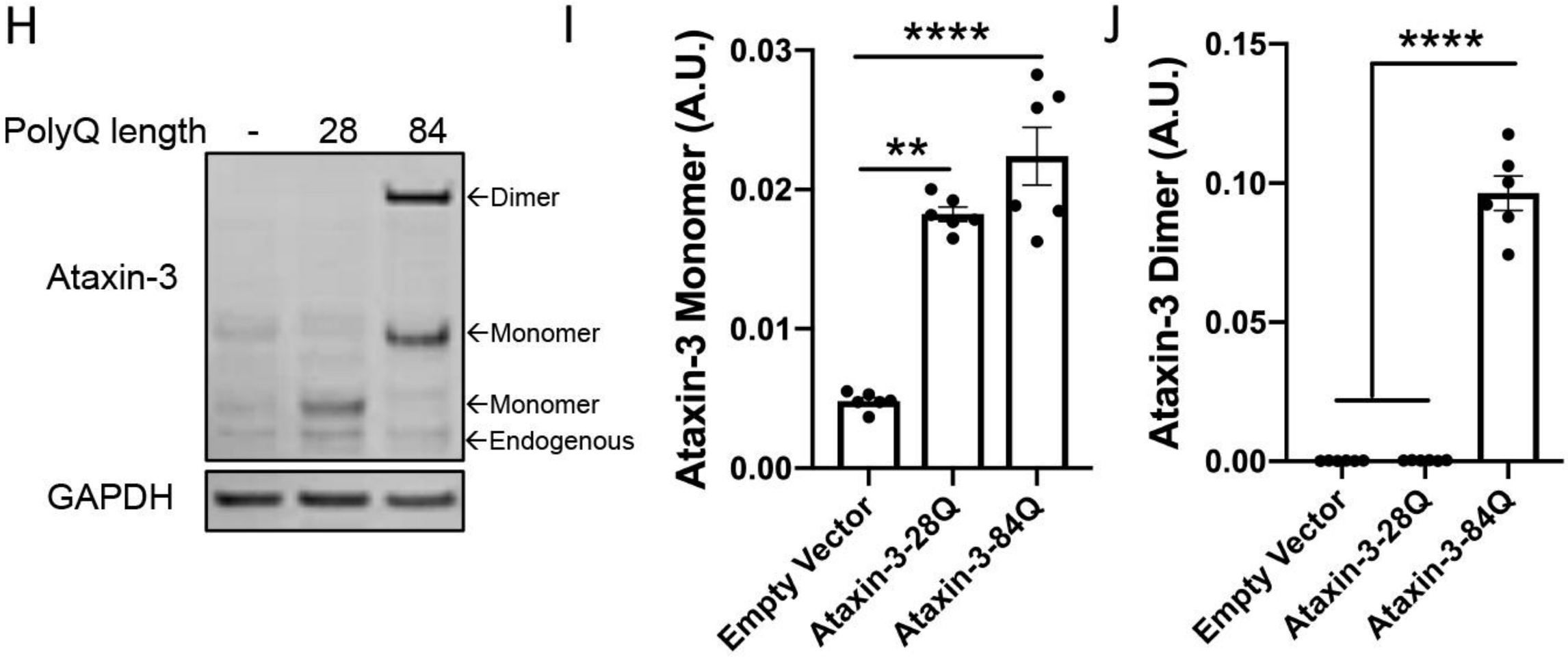

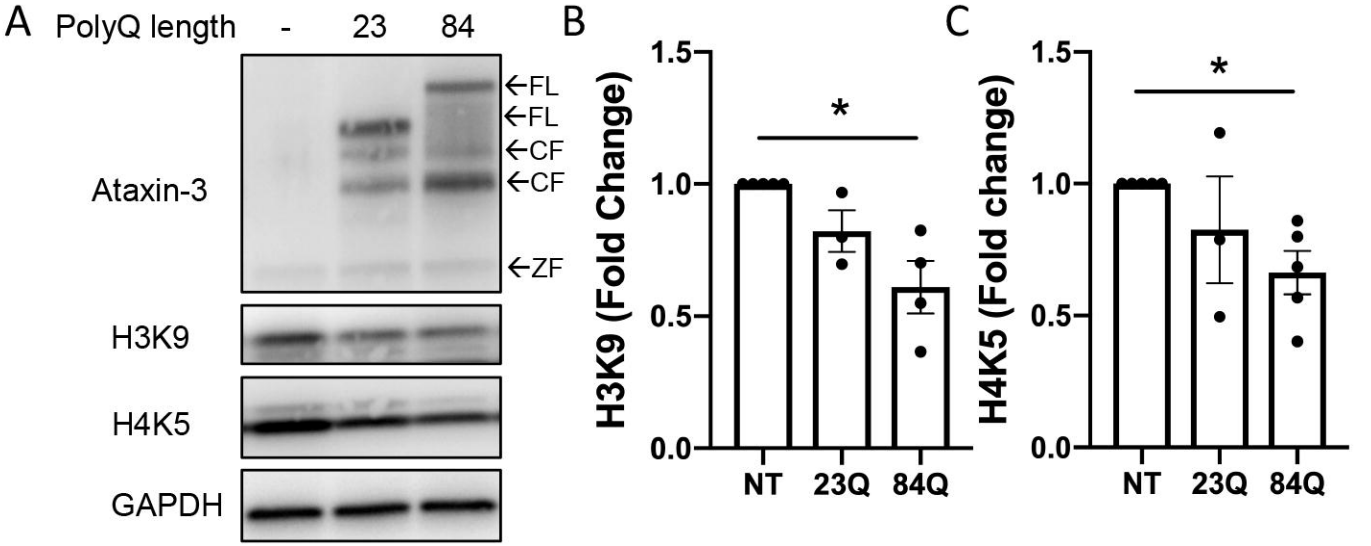
A
PolyQ length
-
23
84
←FL
←FL
←CF
←CF
←ZF
Ataxin-3
H3K9
H4K5
GAPDH
B
H3K9 (Fold Change)
1.5
1.0
0.5
0.0
*
NT
23Q
84Q
C
H4K5 (Fold change)
1.5
1.0
0.5
0.0
*
NT
23Q
84Q

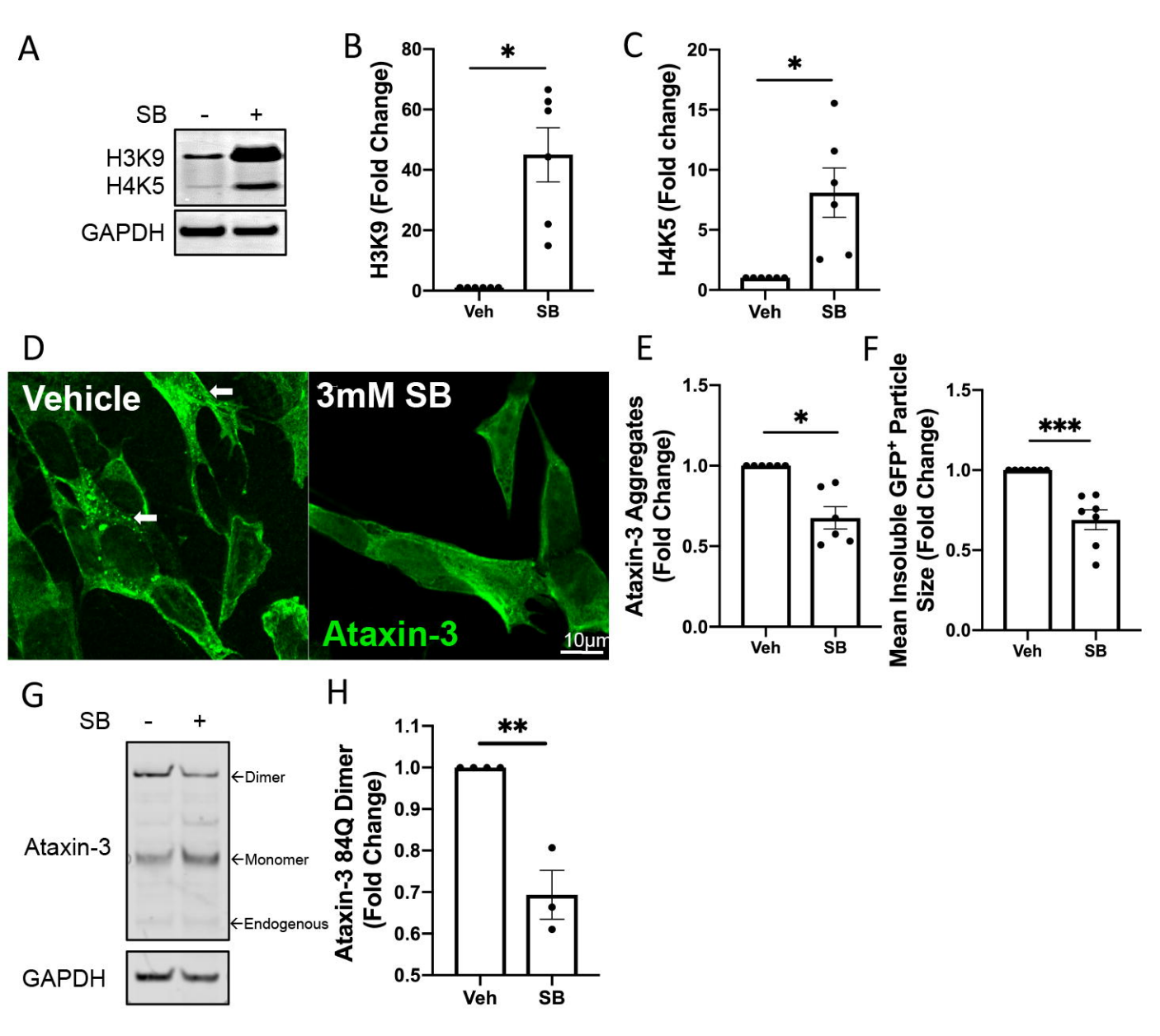
A
SB - +
H3K9
H4K5
GAPDH
B
H3K9 (Fold Change)
80
60
40
20
0
*
Veh
SB
C
H4K5 (Fold change)
20
15
10
5
0
*
Veh
SB
D
Vehicle
3mM SB
Ataxin-3
10μm
E
Ataxin-3 Aggregates (Fold Change)
1.5
1.0
0.5
0.0
*
Veh
SB
F
Mean Insoluble GFP+ Particle Size (Fold Change)
1.5
1.0
0.5
0.0
***
Veh
SB
G
SB - +
Ataxin-3
←Dimer
←Monomer
←Endogenous
GAPDH
H
Ataxin-3 84Q Dimer (Fold Change)
1.1
1.0
0.9
0.8
0.7
0.6
0.5
**
Veh
SB

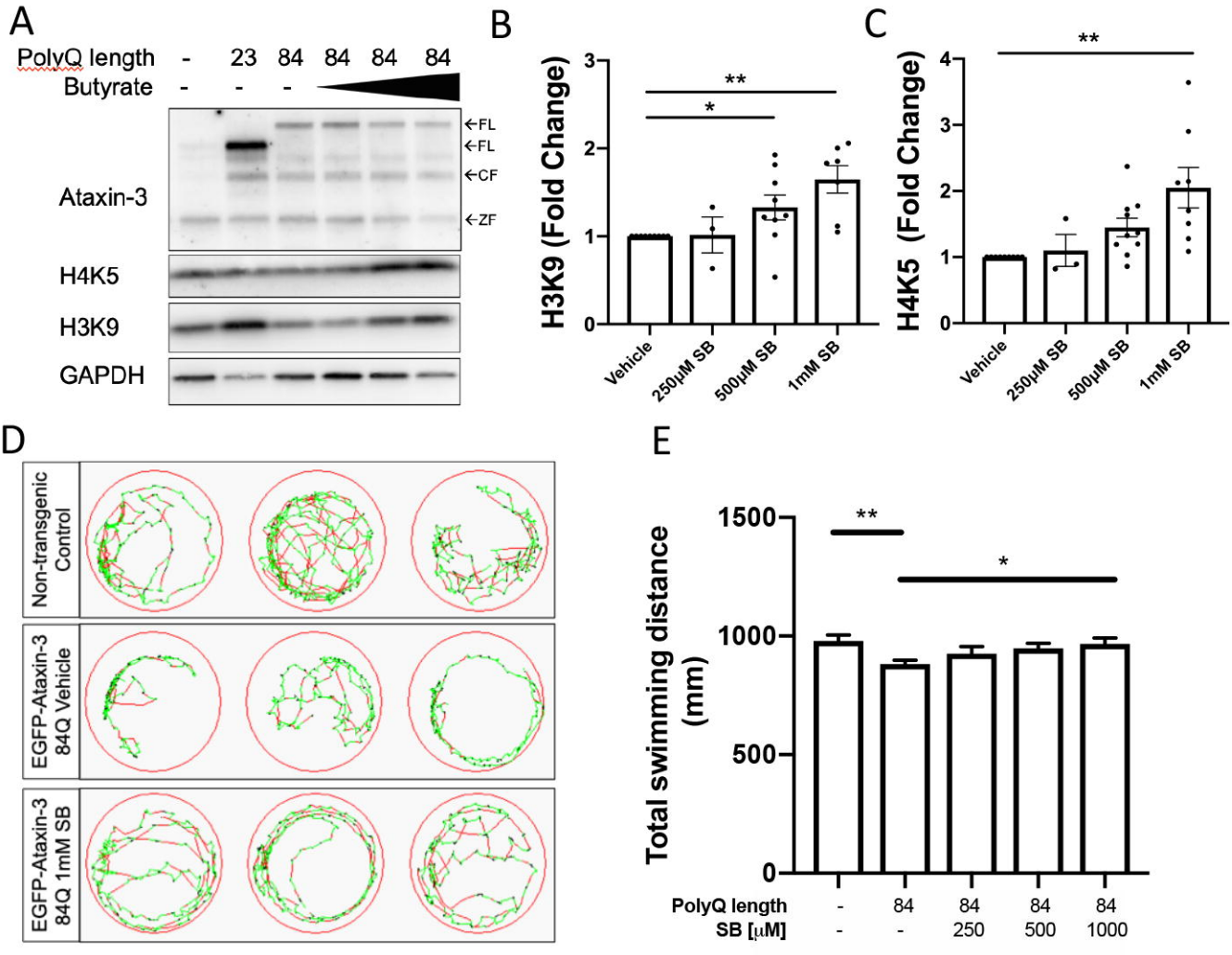
A
PolyQ length - 23 84 84 84 84
Butyrate - - - ▲
Ataxin-3
←FL
←FL
←CF
←ZF
H4K5
H3K9
GAPDH
B
H3K9 (Fold Change)
0
1
2
3
**
*
Vehicle
250μM SB
500μM SB
1mM SB
C
H4K5 (Fold Change)
0
1
2
3
4
**
Vehicle
250μM SB
500μM SB
1mM SB
D
Non-transgenic Control
EGFP-Ataxin-3 84Q Vehicle
EGFP-Ataxin-3 84Q 1mM SB
E
Total swimming distance (mm)
0
500
1000
1500
**
*
PolyQ length - 84 84 84 84
SB [μM] - - 250 500 1000

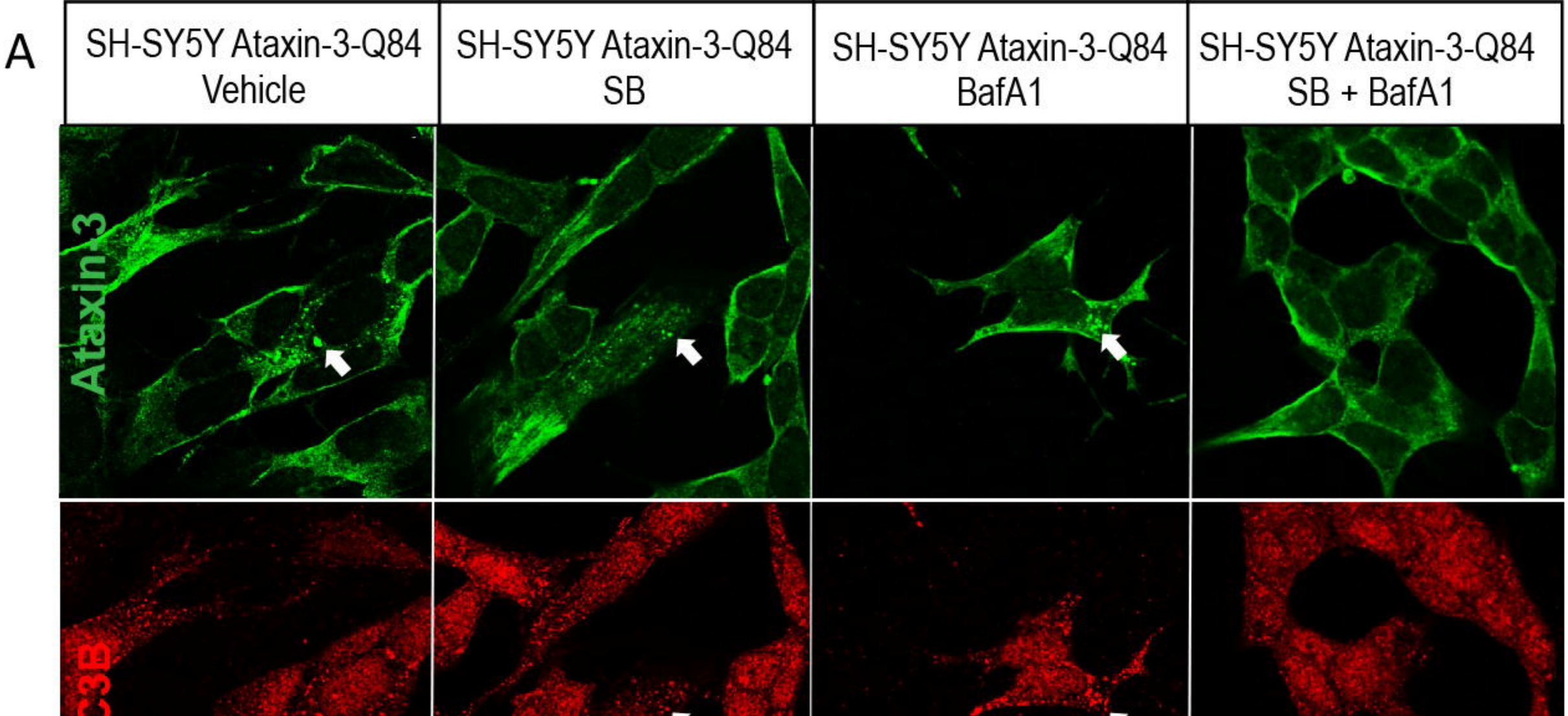

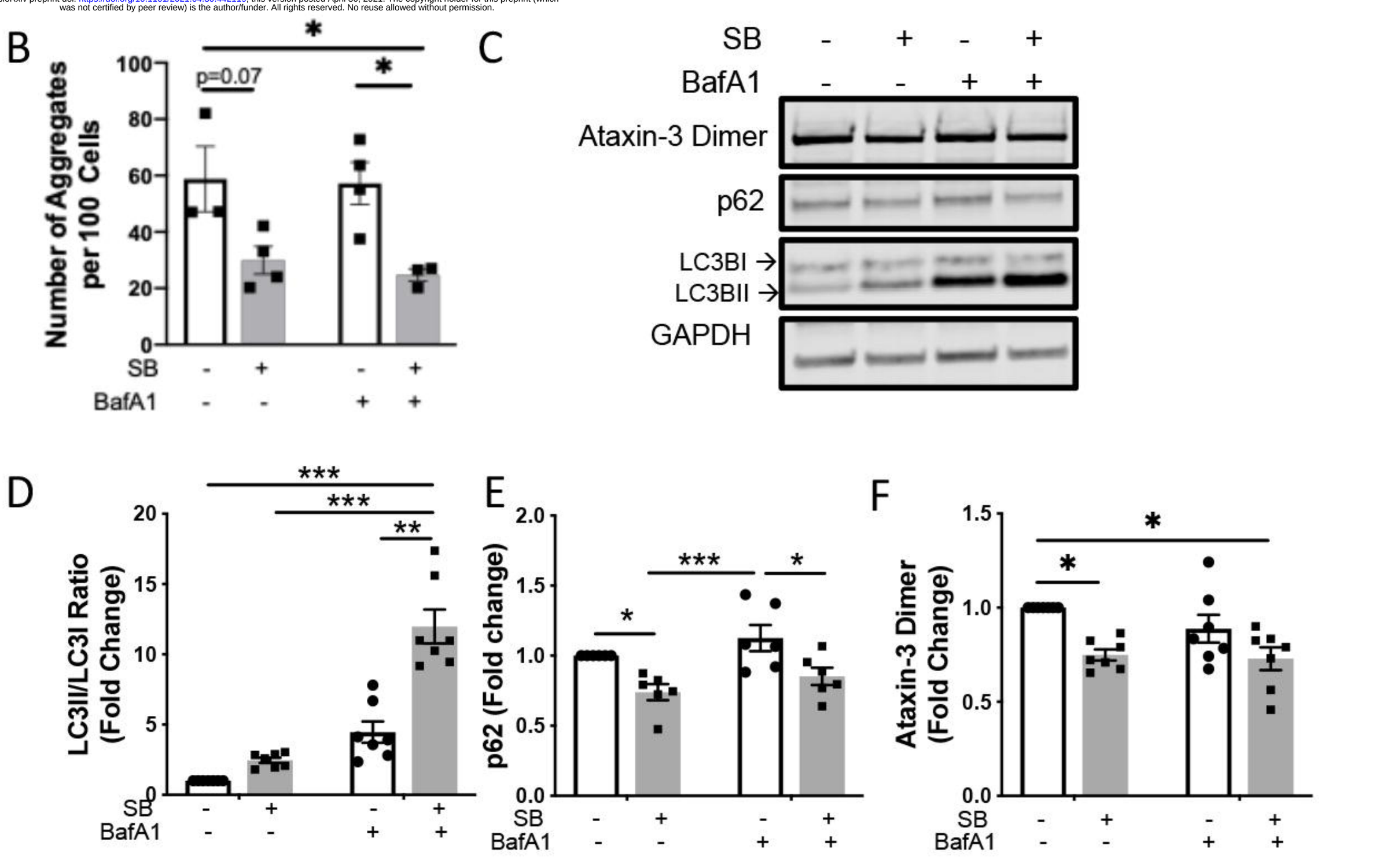

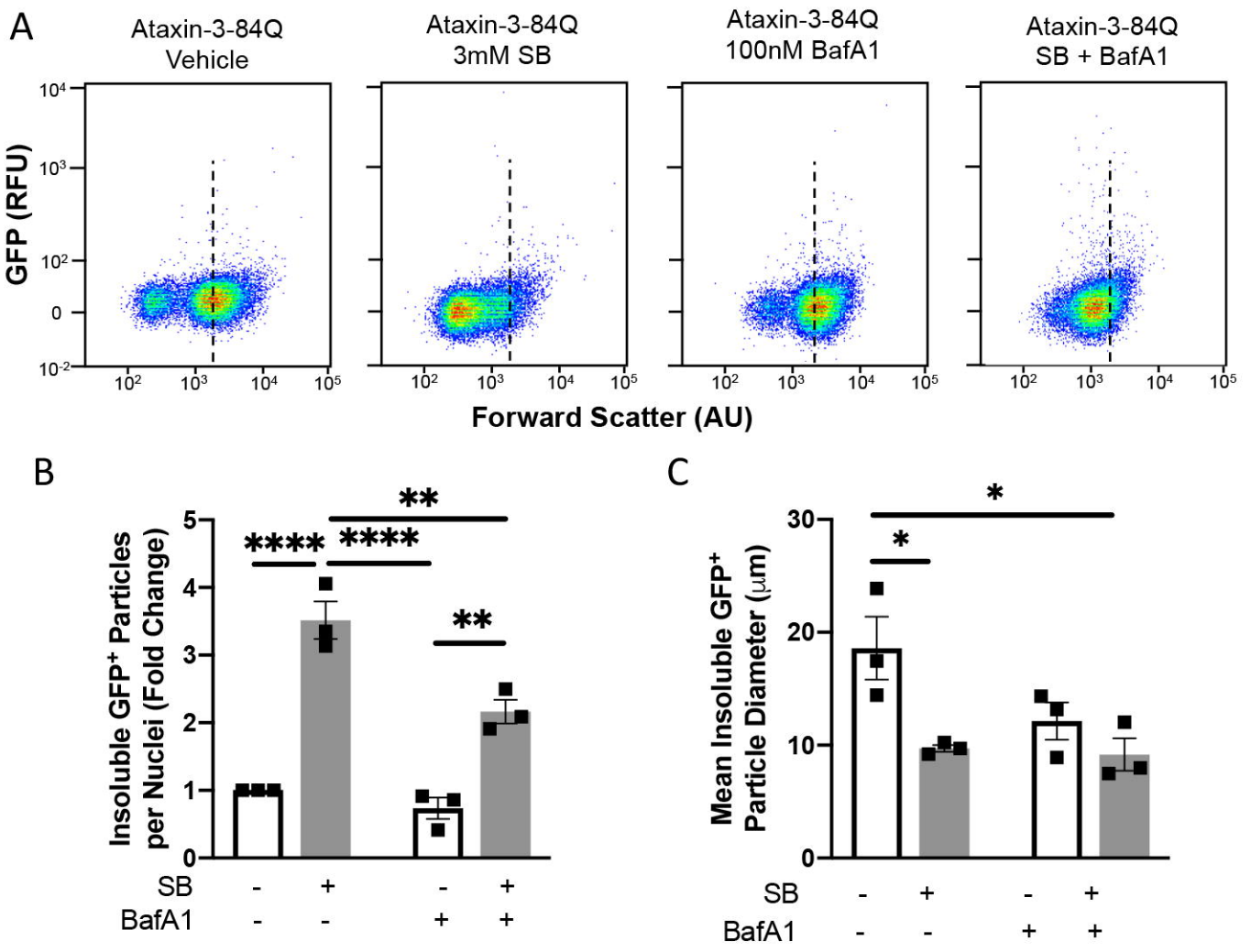
A
Ataxin-3-84Q
Vehicle
Ataxin-3-84Q
3mM SB
Ataxin-3-84Q
100nM BafA1
Ataxin-3-84Q
SB + BafA1
GFP (RFU)
Forward Scatter (AU)
B
Insoluble GFP+ Particles
per Nuclei (Fold Change)
SB
BafA1
C
Mean Insoluble GFP+
Particle Diameter (μm)
SB
BafA1

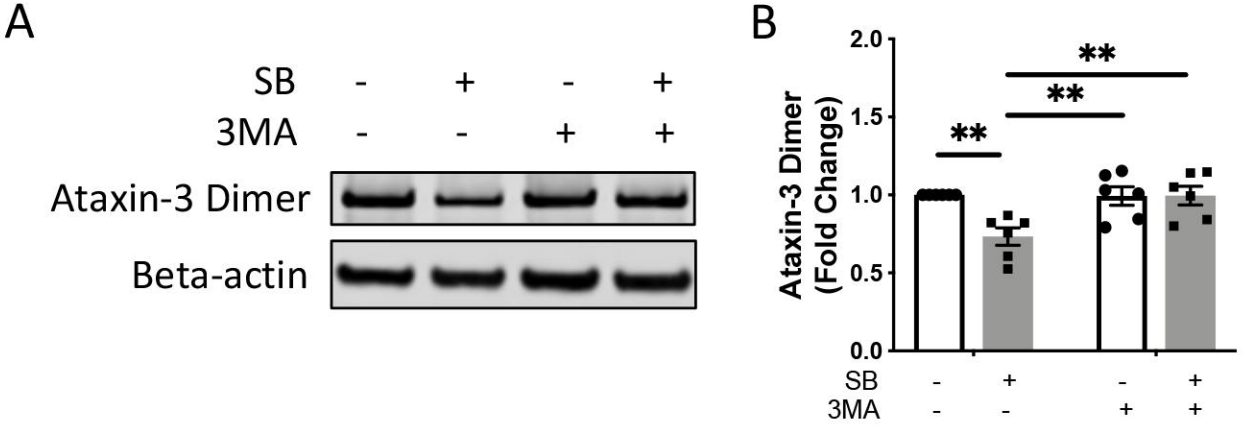
A
SB - + - +
3MA - - + +
Ataxin-3 Dimer
Beta-actin
B
Ataxin-3 Dimer (Fold Change)
2.0
1.5
1.0
0.5
0.0
**
**
**
SB - + - +
3MA - - + +

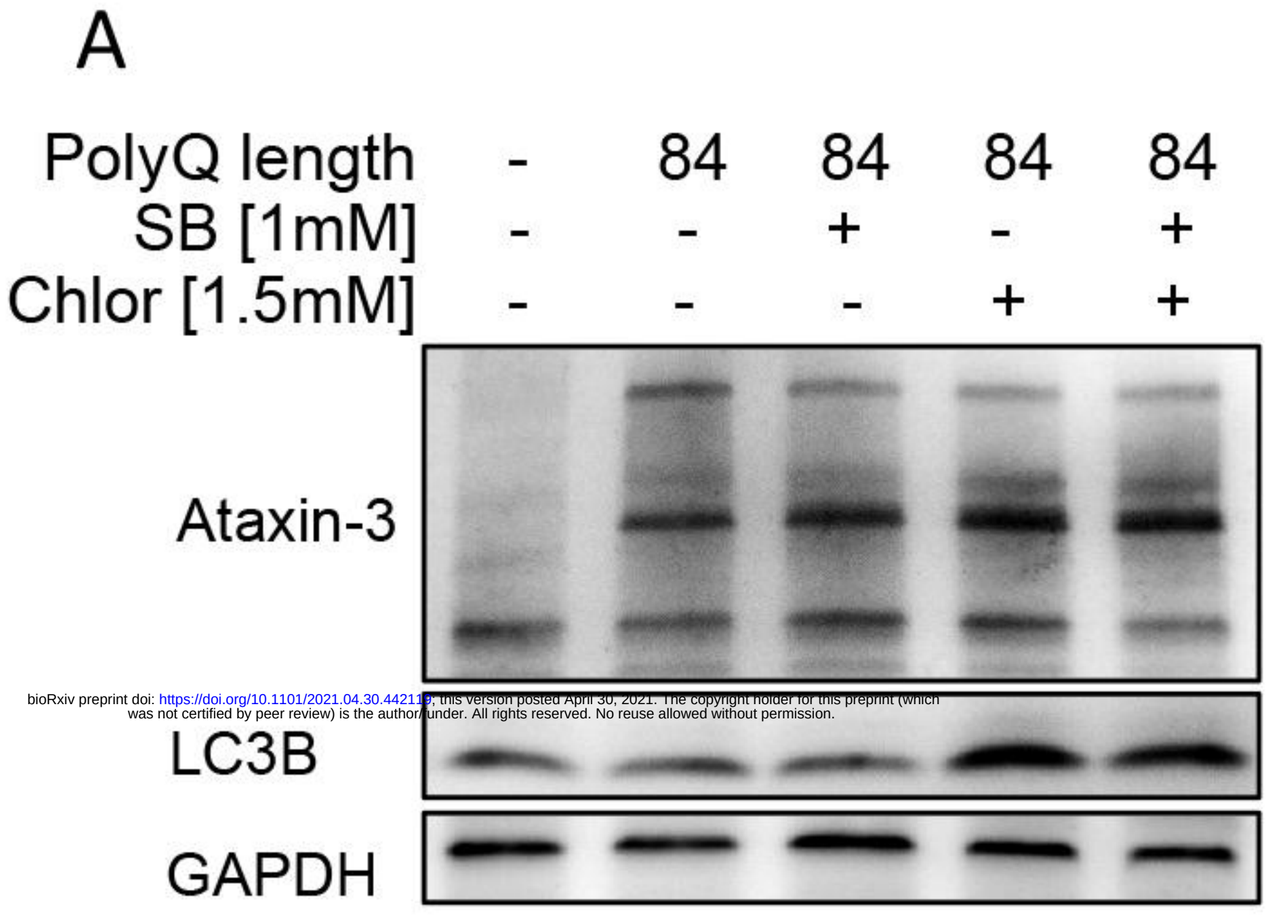

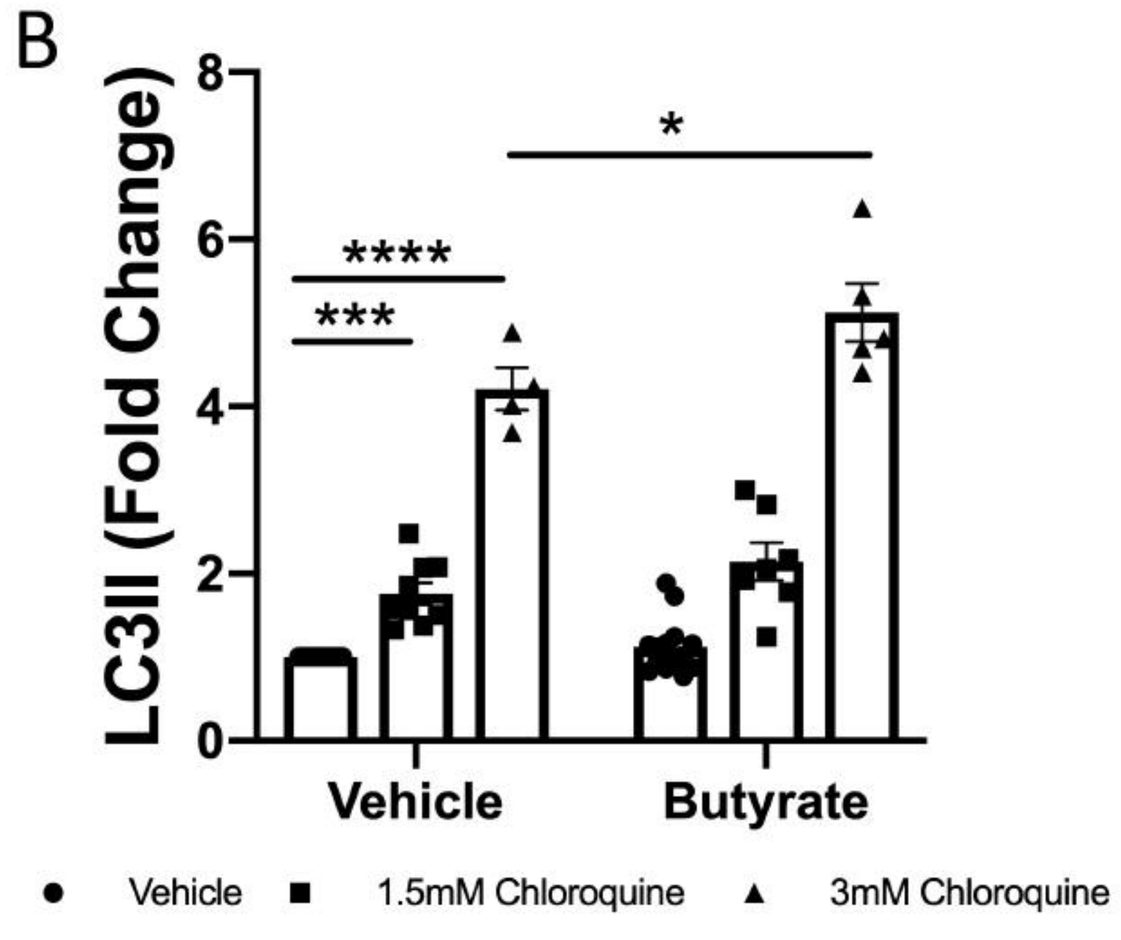

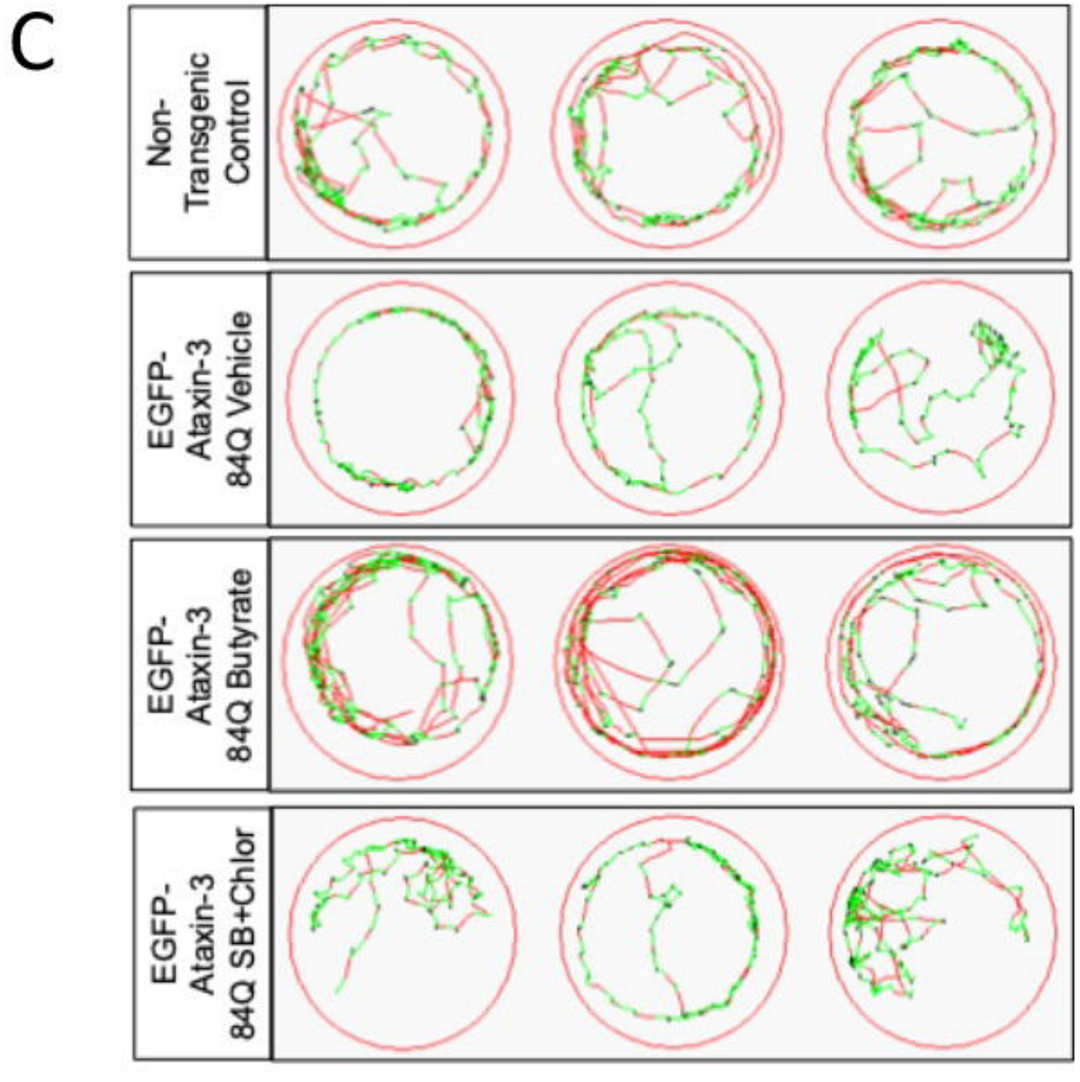

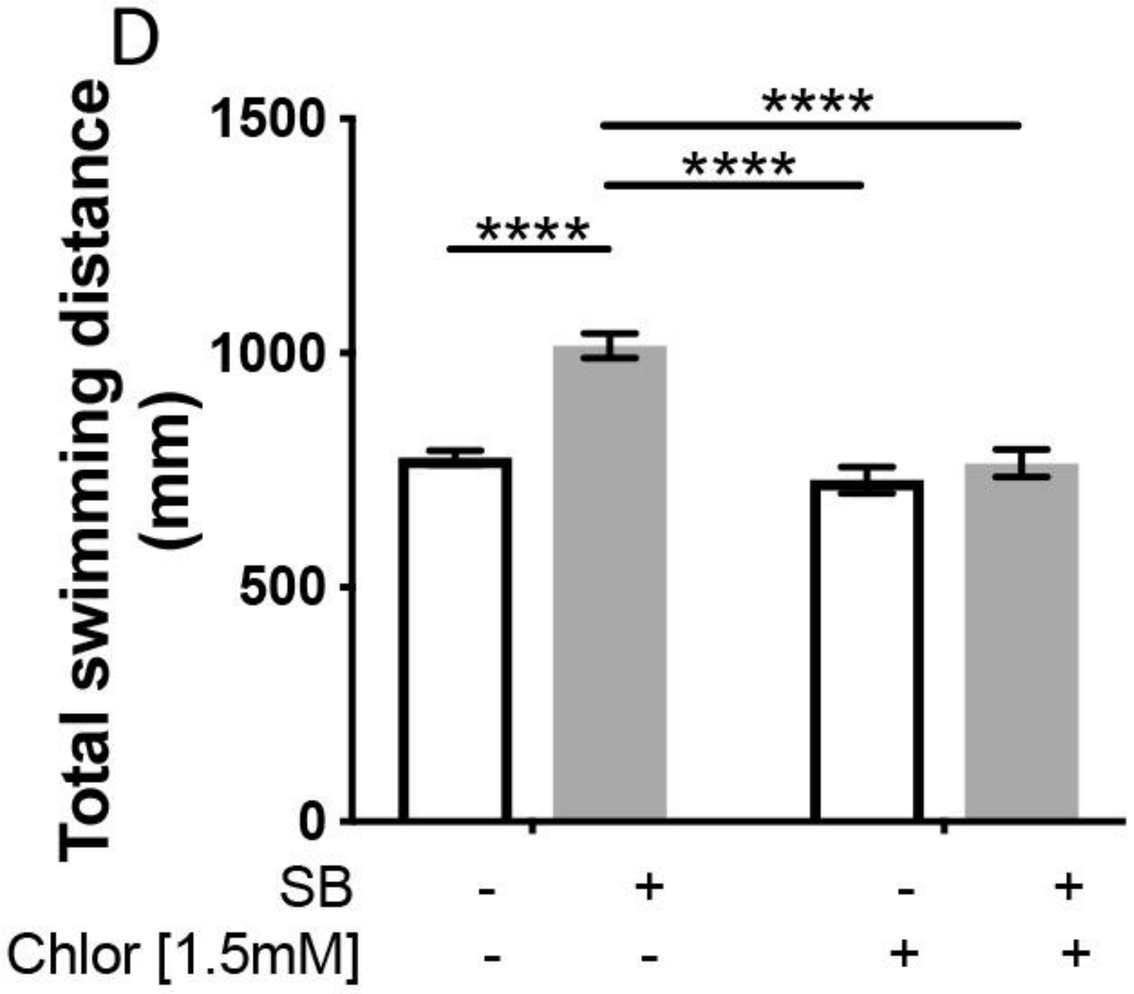

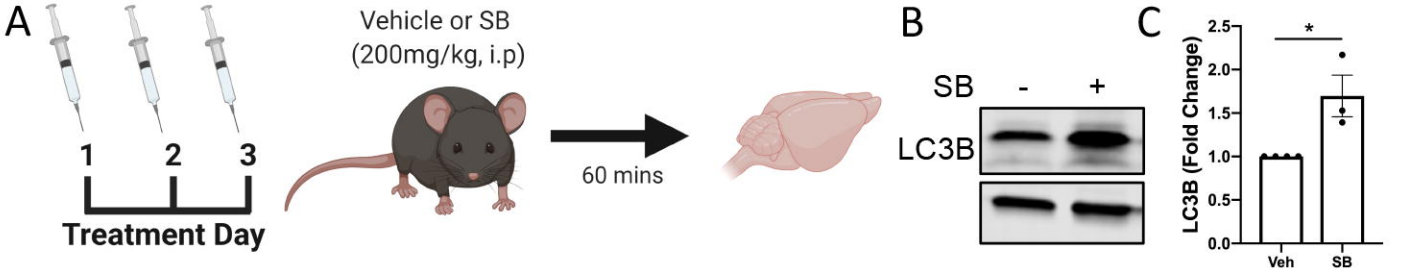
A
1
2
3
Treatment Day
Vehicle or SB
(200mg/kg, i.p)
60 mins
B
SB
-
+
LC3B
C
LC3B (Fold Change)
2.5
2.0
1.5
1.0
0.5
0.0
*
Veh
SB

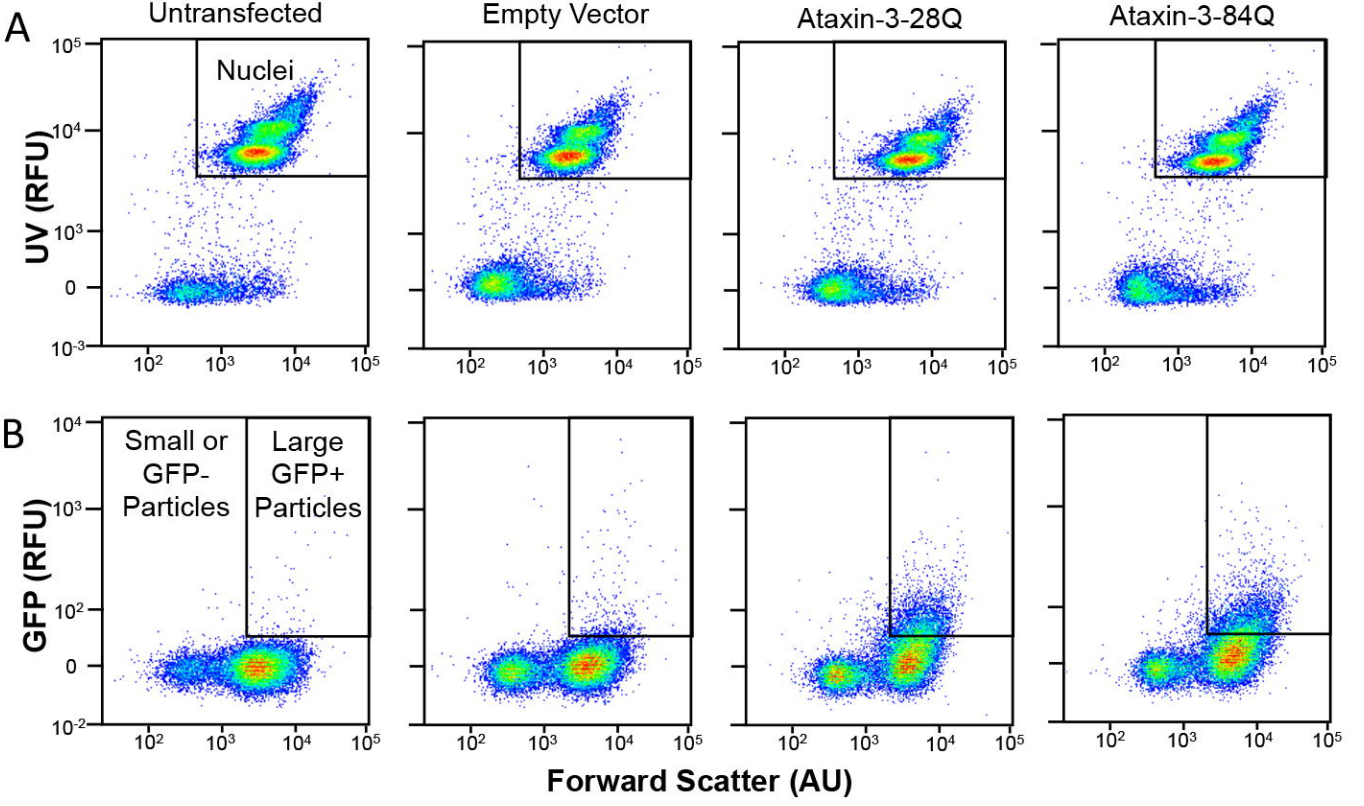
A
Untransfected
Empty Vector
Ataxin-3-28Q
Ataxin-3-84Q
Nuclei
UV (RFU)
B
Small or GFP- Particles
Large GFP+ Particles
GFP (RFU)
Forward Scatter (AU)

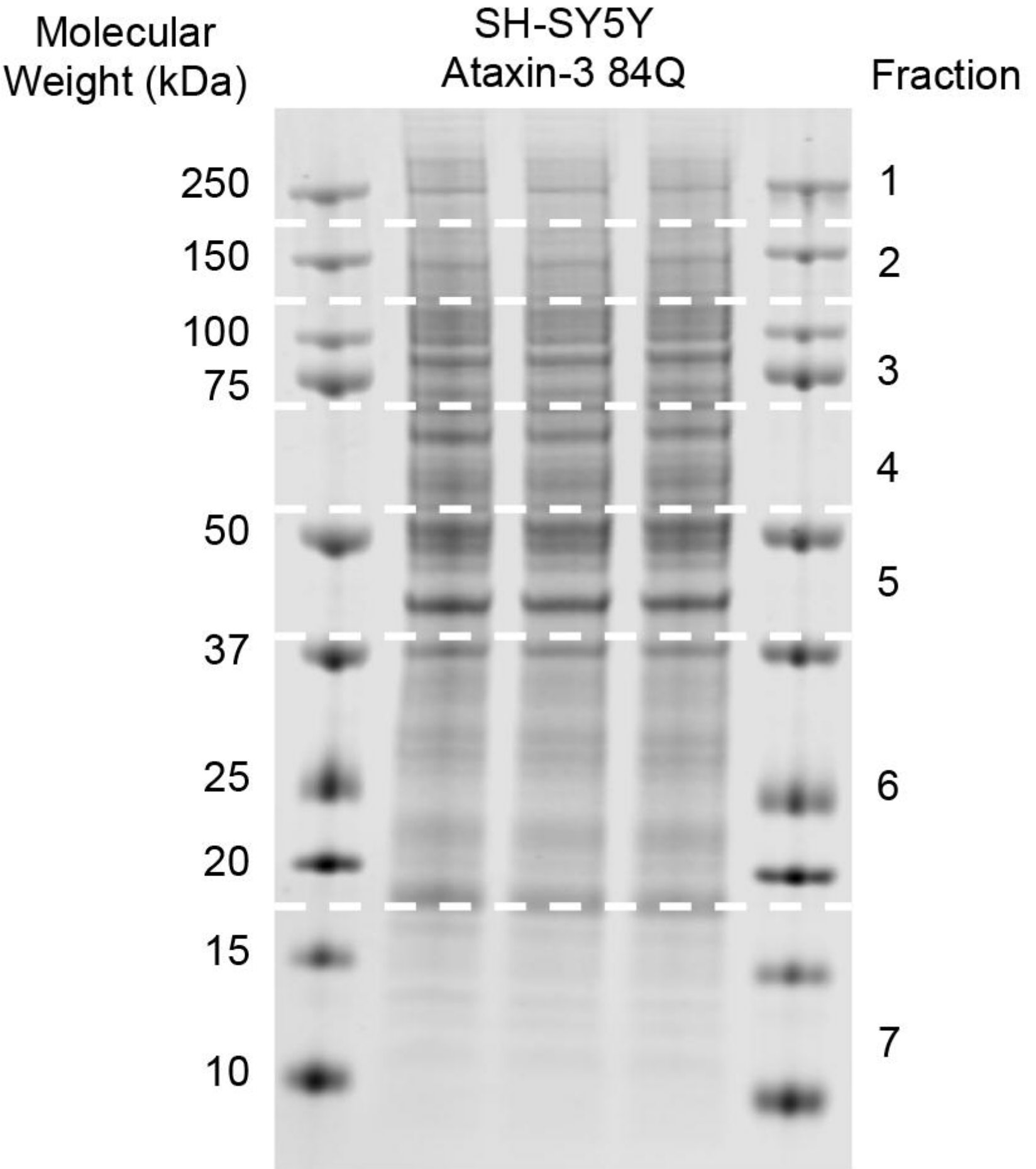
Molecular Weight (kDa)
SH-SY5Y Ataxin-3 84Q
Fraction
250
150
100
75
50
37
25
20
15
10
1
2
3
4
5
6
7

Fraction#2

Protein F	Accession	Description	Exp. q-value:	Sum PEP Scor	Coverage [%]	# Peptide	# PSMs	# Unique	MW [kD	calc. pI	Score Seque	# Peptides (	Gene Symbo	# Protein Groups
High	P54252	Ataxin-3 [OS=Homo sapi	0	101.525	33	10	74	10	41.8	4.91	227.38	10	ATXN3	1
	Confidence	Sequence	Modifications	Qvality PEP	Qvality q-val	# Protein	# Protein	# PSMs	Master	# Missec	Theo. MH+ [	Percolator c	Percolator P	XCorr (by Search Engine): Sequest HT
	High	LIGEELAQLKEQR		0.0000501	0.00011296	1	5	7	P54252	1	1526.8537	6.993E-05	6.245E-06	3.37
	High	LIGEELAQLK		0.00029141	0.00011296	1	5	9	P54252	0	1113.6514	6.993E-05	5.029E-05	2.17
	High	MAEGGVTSEDYR		3.1435E-05	0.00011296	1	3	7	P54252	0	1314.5631	6.993E-05	3.606E-06	3.57
	High	MAEGGVTSEDYR	1xOxidation [	0.00010421	0.00011296	1	3	6	P54252	0	1330.558	6.993E-05	1.485E-05	3.02
	High	QEIDMEDEEADLRR		0.00034291	0.00011296	1	5	4	P54252	1	1748.7756	6.993E-05	0.0000611	3.7
	High	NISQDMTQTSGTNLTSEE	1xOxidation [	1.2416E-07	0.00011296	1	5	3	P54252	1	2369.1249	6.993E-05	5.137E-09	4.31
	High	NISQDMTQTSGTNLTSEE		1.3119E-09	0.00011296	1	5	4	P54252	1	2353.13	6.993E-05	2.328E-11	5.87
	High	NISQDMTQTSGTNLTSEE		3.2889E-10	0.00011296	1	5	6	P54252	0	2225.035	6.993E-05	4.533E-12	6.9
	High	AIQLSMQGSSR	1xOxidation [	0.00206702	0.00011296	1	5	5	P54252	0	1193.5943	6.993E-05	0.0005122	2.91
	High	AIQLSMQGSSR		0.00197743	0.00011296	1	5	6	P54252	0	1177.5994	6.993E-05	0.0004853	2.52
	High	GDLPDCEADQLLQMIR	1xCarbamido	5.3638E-06	0.00011296	1	4	10	P54252	0	1873.8783	6.993E-05	4.445E-07	4.88
	High	QEIDMEDEEADLRR	1xOxidation [	0.00372979	0.00023499	1	5	2	P54252	1	1764.7705	0.000112	0.001037	2.12
	High	TFLQQPSGNMDDSGFFSI		0.00567507	0.00023499	1	2	1	P54252	0	2844.3873	0.000112	0.001701	4.19
	High	IDPINER		0.0372436	0.00135453	1	4	3	P54252	0	856.45231	0.0008518	0.0161	1.48
	High	GDLPDCEADQLLQMIR	1xCarbamido	0.113736	0.00461755	1	4	1	P54252	0	1889.8732	0.002625	0.06271	2.62

Fraction #3

Protein F	Accession	Description	Exp. q-value:	Sum PEP Scor	Coverage [%]	# Peptide	# PSMs	# Unique	MW [kD	calc. pI	Score Seque	# Peptides (	Gene Symbo	# Protein Groups
High	P54252	Ataxin-3 [OS=Homo sapi	0	11.709	9	3	4	3	41.8	4.91	10.92	3	ATXN3	1
	Confidence	Sequence	Modifications	Qvality PEP	Qvality q-val	# Protein	# Protein	# PSMs	Master	# Missec	Theo. MH+ [	Percolator c	Percolator P	XCorr (by Search Engine): Sequest HT
	High	MAEGGVTSEDYR		0.00019502	0.00016268	1	3	2	P54252	0	1314.5631	8.205E-05	2.998E-05	3.34
	High	LIGEELAQLK		0.00046257	0.00016268	1	5	1	P54252	0	1113.6514	8.205E-05	0.0000834	1.99
	High	AIQLSMQGSSR		0.00304566	0.00016268	1	5	1	P54252	0	1177.5994	8.205E-05	0.000781	2.23

Fraction #4

Protein F	Accession	Description	Exp. q-value:	Sum PEP Scor	Coverage [%]	# Peptide	# PSMs	# Unique	MW [kD	calc. pI	Score Seque	# Peptides (	Gene Symbo	# Protein Groups
High	P54252	Ataxin-3 [OS=Homo sapi	0	34.909	21	6	18	6	41.8	4.91	61.99	6	ATXN3	1
	Confidence	Sequence	Modifications	Qvality PEP	Qvality q-val	# Protein	# Protein	# PSMs	Master	# Missec	Theo. MH+ [	Percolator c	Percolator P	XCorr (by Search Engine): Sequest HT
	High	QEIDMEDEEADLRR		0.00052077	0.00014104	1	5	2	P54252	1	1748.7756	5.778E-05	0.0000696	3.88
	High	NISQDMTQTSGTNLTSEE		5.6986E-05	0.00014104	1	5	1	P54252	1	2353.13	5.778E-05	4.551E-06	2.84
	High	LIGEELAQLKEQR		0.00024401	0.00014104	1	5	4	P54252	1	1526.8537	5.778E-05	2.727E-05	3.65
	High	LIGEELAQLK		0.00253869	0.00014104	1	5	3	P54252	0	1113.6514	5.778E-05	0.0004911	2.74
	High	MAEGGVTSEDYR	1xOxidation [	0.00187542	0.00014104	1	3	1	P54252	0	1330.558	5.778E-05	0.0003383	2.78
	High	MAEGGVTSEDYR		6.7238E-05	0.00014104	1	3	3	P54252	0	1314.5631	5.778E-05	5.563E-06	3.91
	High	GDLPDCEADQLLQMIR	1xCarbamido	0.00015166	0.00014104	1	4	4	P54252	0	1873.8783	5.778E-05	1.516E-05	3.99

Fraction #5

Protein F	Accession	Description	Exp. q-value:	Sum PEP Scor	Coverage [%]	# Peptide	# PSMs	# Unique	MW [kD	calc. pI	Score Seque	# Peptides (	Gene Symbo	# Protein Groups
High	P54252	Ataxin-3 [OS=Homo sapi	0	5.683	6	2	3	2	41.8	4.91	5.43	2	ATXN3	1
	Confidence	Sequence	Modifications	Qvality PEP	Qvality q-val	# Protein	# Protein	# PSMs	Master	# Missec	Theo. MH+ [	Percolator c	Percolator P	XCorr (by Search Engine): Sequest HT
	High	MAEGGVTSEDYR		0.00148559	0.0004731	1	3	2	P54252	0	1314.5631	0.0001662	0.0001989	2.68
	High	LIGEELAQLK		0.0353396	0.00064657	1	5	1	P54252	0	1113.6514	0.0002615	0.01043	1.36

Fraction #6

Protein F	Accession	Description	Exp. q-value:	Sum PEP Scor	Coverage [%]	# Peptide	# PSMs	# Unique	MW [kD	calc. pI	Score Seque	# Peptides (	Gene Symbo	# Protein Groups
High	P54252	Ataxin-3 [OS=Homo sapi	0	3.982	3	1	1	1	41.8	4.91	2.63	1	ATXN3	1
	Confidence	Sequence	Modifications	Qvality PEP	Qvality q-val	# Protein	# Protein	# PSMs	Master	# Missec	Theo. MH+ [	Percolator c	Percolator P	XCorr (by Search Engine): Sequest HT
	High	MAEGGVTSEDYR		0.00097991	0.00014741	1	3	1	P54252	0	1314.5631	5.494E-05	0.0001043	2.63

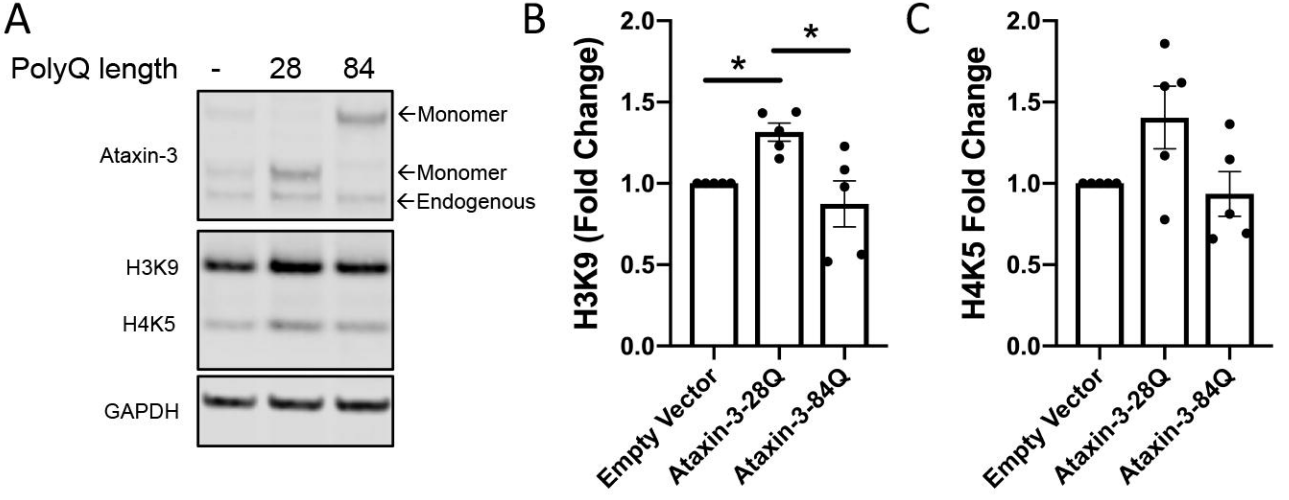
A
PolyQ length
-
28
84
Ataxin-3
←Monomer
←Monomer
←Endogenous
H3K9
H4K5
GAPDH
B
H3K9 (Fold Change)
2.0
1.5
1.0
0.5
0.0
*
*
Empty Vector
Ataxin-3-28Q
Ataxin-3-84Q
C
H4K5 Fold Change
2.0
1.5
1.0
0.5
0.0
Empty Vector
Ataxin-3-28Q
Ataxin-3-84Q

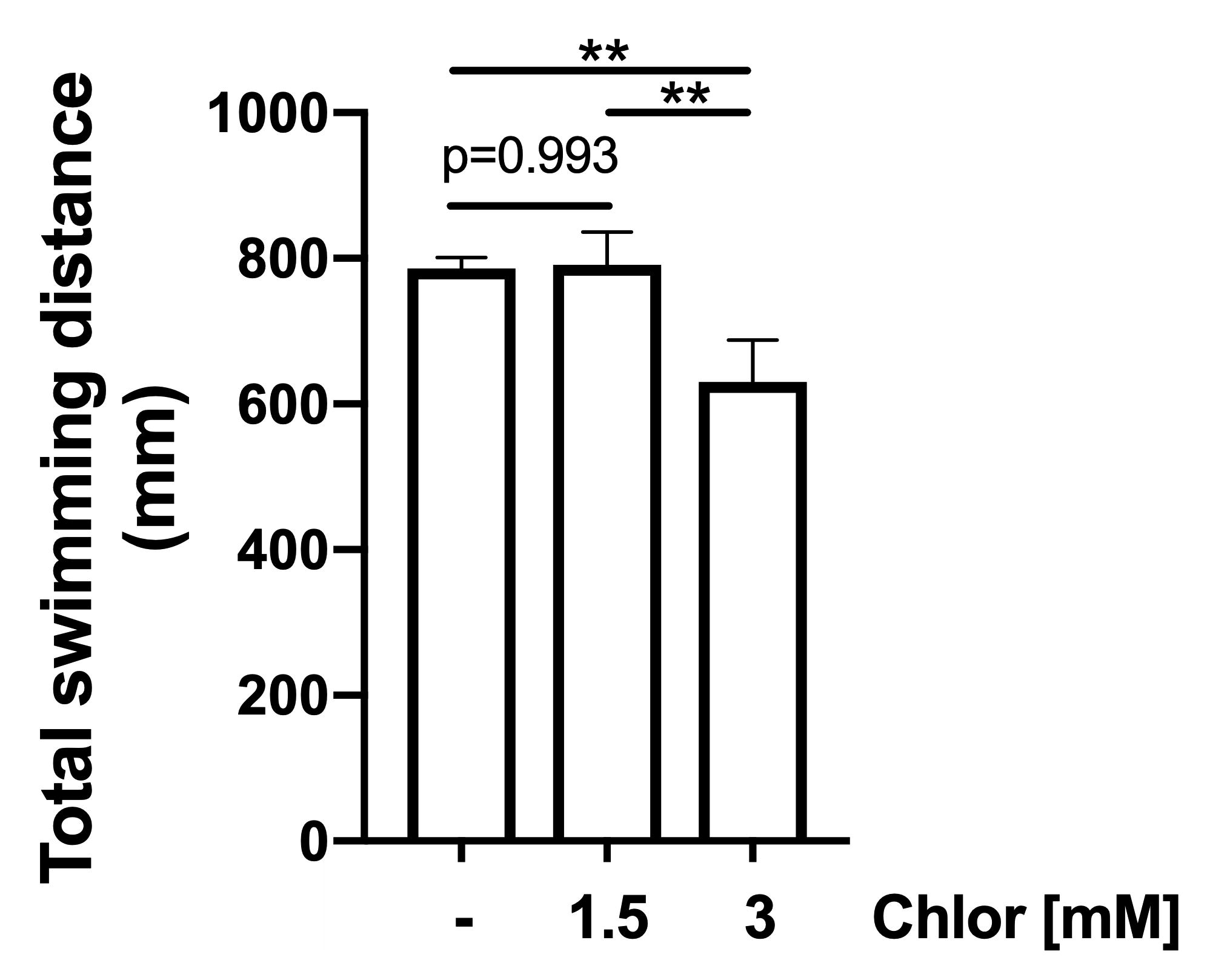
**
**
p=0.993
1000
800
600
400
200
0
Total swimming distance (mm)
-
1.5
3
Chlor [mM]